Scientific Research Publishing

Journal of Applied Mathematics and Physics, 2026, 14(4), 1535-1586
https://www.scirp.org/journal/jamp
ISSN Online: 2327-4379
ISSN Print: 2327-4352

Quantum Mechanics of the Timeon Field: Algebraic and Symplectic Framework for Quantum Gravity

George Davey

Independent Researcher, West Des Moines, IA, USA
Email: George.Davey@QuantumLinear.com

How to cite this paper: Davey, G. (2026) Quantum Mechanics of the Timeon Field: Algebraic and Symplectic Framework for Quantum Gravity. *Journal of Applied Mathematics and Physics*, **14**, 1535-1586.
https://doi.org/10.4236/jamp.2026.144073

Received: March 13, 2026
Accepted: April 19, 2026
Published: April 22, 2026

Abstract

We develop a comprehensive quantum-mechanical and field-theoretic framework for a complex scalar field whose modulus encodes a local time density and whose internal phase carries a $U(1)$ structure. This field, which we call the *timeon*, admits a potential with two thermodynamically distinct minima: a null-stress vacuum phase and a deeper condensed, highly stable atomic phase. We show that localised, finite-energy atomic-phase domains embedded within the vacuum couple naturally to a conventional matter wavefunction $\psi(\boldsymbol{x},t)$, giving rise to a new class of composite eigenstates—*Baryon Partner States* (BPS). These states are elements of the composite Hilbert space $\mathcal{H}_{\psi}\otimes\mathcal{H}_{\Phi}$ and function as the fundamental excitations of the theory. We derive the complete Lagrangian and Hamiltonian governing the timeon field, obtain the coupled Euler-Lagrange equations for the composite system, and construct static, spherically symmetric BPS configurations satisfying regularity and finite-energy boundary conditions. Each BPS exhibits a topologically constrained core, a nontrivial radial profile, and a quantised $U(1)$ phase winding. These structures endow the states with emergent mass, charge, and confinement properties. Baryonic mass arises entirely from spatial gradients and potential energy of the field configuration; charge originates from the internal phase winding; and confinement emerges as an energetic and geometric necessity—continuous unwinding of the phase is forbidden without traversal of configurations carrying arbitrarily large energy cost, preventing fractional excitations from existing in isolation. Vacuum-to-atomic tunnelling and atomic-phase nucleation processes are analysed in detail, including energy barriers, critical radii, and transition amplitudes for metastable decay. The local matter density $|\psi|^2$ acts as a compression parameter that dynamically lowers nucle-

ation thresholds and drives the formation of atomic-phase regions. Linearization about both homogeneous phases and static BPS configurations yields the complete small-oscillation spectrum of the theory; these internal modes form a predictive excitation tower and correspond directly to resonances in scattering processes. By promoting the translational degree of freedom of a BPS to a dynamical modulus, we derive its effective nonrelativistic Lagrangian and identify a renormalized inertial mass. Pairwise interactions between BPSs generate an effective potential consisting of strong short-range repulsion, an intermediate-range attractive well, and Yukawa-like long-range decay. This structure supports two-body bound states, determines low-energy scattering phase shifts, and produces resonances when collision energies match internal excitation frequencies. Extending to many-body systems, we show that BPSs form stable clusters analogous to small nuclei. A systematic low-energy effective field theory is obtained by integrating out internal BPS modes. Together, these results demonstrate that mass, charge, confinement, excitation spectra, scattering behaviour, and nuclear-like structure can emerge from the dynamics of a single complex field coupled to a matter wavefunction.

Keywords

Quantum Gravity, Baryon Partner State, Timeon Lattice Potential (TLP), Time Density, Chrono-Quantum Mirror (CQM), Chrono-Shear Event, Quantum Mechanics, Timeon Lattice, Matter Formation, Scattering Theory, Mass-Energy Conversion

1. Introduction

In conventional quantum field theory, quantum fields are excitations of a dynamical medium defined over a spacetime background, and the vacuum is the lowest-energy eigenstate of the Hamiltonian—not an independent entity. General relativity treats the metric itself as dynamical, sourced by stress-energy. We do not contest any of this. The point of departure of the present work is more specific: in both frameworks, the spacetime metric $g_{\mu\nu}$ enters as a *prior* structure—either a fixed background in QFT or a field governed by Einstein's equations in GR—and matter, radiation, and gravitational dynamics are built upon it. The Timeon framework inverts this causal priority. We posit a single complex scalar field, which we call the *timeon field*, whose amplitude encodes a local *time density* and whose internal phase carries a $U(1)$ structure [1].

Physical meaning of time density. The amplitude $\hat{t}(x)$ is defined operationally as *proper time per unit proper length*:

$$\hat{t}(x) \equiv \left.\frac{\mathrm{d}\tau}{\mathrm{d}l}\right|_x, \quad \left[\hat{t}\right] = \mathrm{s}\cdot\mathrm{m}^{-1}. \tag{1}$$

The quantity $\hat{t}$ is a local, spacetime-varying scalar: regions of strong gravitational curvature, where clocks run slowly relative to distant observers, have higher

$\hat{t}$; asymptotically flat space has $\hat{t} \to \hat{t}_\infty$. Setting $n_t \equiv c\hat{t}$, the *Refractive Postulate*

$$n_t(r) = \frac{n_{t,\infty}}{\sqrt{-g_{tt}(r)}} \tag{2}$$

connects $\hat{t}$ to the metric precisely. For Schwarzschild geometry Equation (2) recovers

$$n_t(r) = n_{t,\infty}\left(1-\frac{2GM}{rc^2}\right)^{-1/2}, \tag{3}$$

which is the standard gravitational time-dilation factor, making $\hat{t}$ measurable in principle through precision clock comparisons. We emphasize that $\hat{t}$ is a *medium parameter*—it encodes how proper time flows per unit proper length—not a time substance subject to its own independent conservation law.

Time Density and the Refractive Postulate: Foundational Summary

Coordinate independence. Both $\mathrm{d}\tau$ and $\mathrm{d}l$ are operationally defined by ideal clocks and rods. Their ratio $\hat{t}$ is therefore a scalar under diffeomorphisms: once a metric is available, $\mathrm{d}\tau^2 = -g_{\mu\nu}u^\mu u^\nu \mathrm{d}\lambda^2$ and $\mathrm{d}l^2 = h_{ij}\mathrm{d}x^i\mathrm{d}x^j$ are tensorial contractions, so $\hat{t}$ is manifestly coordinate-independent.

Physical interpretation. $\hat{t}(x)$ measures the local *clock strain*—the rate at which proper time accumulates per unit spatial extent. In flat spacetime $\hat{t} = \hat{t}_\infty$ uniformly; spatial gradients $\nabla\hat{t} \neq 0$ signal differential clock rates, precisely what an ideal clock measures as gravitational redshift. Curvature is not merely a *symptom* of a non-uniform $\hat{t}$; it is its *consequence*. For Schwarzschild geometry Equation (2) gives

$$n_t(r) = n_{t,\infty}\left(1-\frac{2GM}{rc^2}\right)^{-1/2}, \tag{4}$$

which is the standard gravitational time-dilation factor. The full derivation, including the construction of the metric from $\hat{t}$ alone via two independent pathways (Clock-Induced Geometry and Time-Density Conformal Gravity), is consistent with prior and future work [2].

What is *not* conserved? $\hat{t}$ is a medium parameter—it encodes how proper time flows per unit proper length—not a conserved charge. The quantity that is conserved is the $U(1)$ Noether charge $Q = \int j^0 \mathrm{d}^3x$, where $j^\mu = 2\hat{t}^2\partial^\mu\theta$ is the current generated by the phase symmetry $\Phi \to \mathrm{e}^{i\alpha}\Phi$ (derived in **Appendix C**). This distinction is maintained throughout the paper. This charge is the topological winding number of the BPS configuration and serves as the emergent analogue of baryon number; it is a property of the internal phase θ, not of the amplitude $\hat{t}$. The full derivation of Equation (2) and its observational consequences are developed in [2]. The central claim is that baryons are not independent elementary objects but stable composite configurations formed by the interaction between this time-density field and a conventional matter wavefunction. At the level of classical field theory, the timeon field $\Phi(x)$ is assumed to have a potential with at least two distinct minima:

- a metastable, low-density *vacuum phase*, and
- a deeper, condensed *atomic phase*.

Spatially localised regions of atomic phase embedded in the vacuum define stable, localised reconfigurations of time density. When these reconfigurations are coupled to an atomic matter wavefunction $\psi(\mathbf{x},t)$, they form what we call *Baryon Partner States* (BPS), in the tensor product Hilbert space:

$$\Psi_{\mathrm{BPS}} \in \mathcal{H}_{\psi} \otimes \mathcal{H}_{\Phi}. \tag{5}$$

The purpose of this paper is to develop the full quantum mechanics of these BPS configurations and to show explicitly how familiar baryonic properties arise from the timeon field. We build upon the foundation of Chrono-Emergence and the Discrete-State Time Density (DTD) framework [2].

Relation to prior "time as field" proposals. Several recent works have explored time as a dynamical field. Ogonowski [3] reformulates the Schwarzschild and Minkowski metrics using a real time-dilation scalar $\Phi = 1/\gamma_r$, showing that both gravitational and electromagnetic fields can be unified through a single time-dilation phenomenon. Fayyaz Malik [4] promotes time to a two-component wave field $\left(T^{+}, T^{-}\right)$ from which mass, charge, and cosmic structure are derived through resonance and micro-Bang dynamics across a series of papers constituting the Time Field Model (TFM). Hart [5] proposes the "Expanding Time Hypothesis," in which the observed cosmic acceleration and redshift are reinterpreted as the expansion of time itself as a scalar field. Hassan *et al.* [6] develop a covariant Temporal Field Theory (TFT) in which a dynamical scalar field $\mathcal{T}\left(x^{\mu}\right)$ sourced by entropy and information flux predicts "chronocurvature" and "chronotension"—spatial non-uniformities in time flow.

The present work differs from all of these in three respects. First, the timeon field $\Phi = \hat{t}\,\mathrm{e}^{i\theta}$ is *complex*, admitting a $U(1)$ internal symmetry whose Noether charge becomes the topological invariant labelling stable baryonic states; no prior time-field model possesses this internal structure. Second, the timeon Lagrangian supports *discrete phase transitions*: the field inhabits a low-density vacuum phase below $\hat{t}_{\mathrm{crit}}$ and a dense-time phase above it, and the BPS soliton emerges precisely because its spatial profile interpolates between these two phases, creating a mass gap. Third, *matter formation* is predicted endogenously: the BPS is a localised, topological, highly stable excitation of the timeon field itself, not matter placed in a time-field background.

2. Composite Hilbert Space and BPS Conceptual Overview

The first step toward a quantum description of baryons in the timeon framework is to formalize the joint Hilbert space on which both the matter wavefunction and the timeon field act. In this section we define the composite space, construct the corresponding Hamiltonian operators, and identify the Baryon Partner State (BPS) as a joint eigenstate of the full Hamiltonian.

Functional Setting. Unless otherwise specified, all fields are assumed to lie in a

separable complex Hilbert space $\mathcal{H}$ with inner product $\langle \cdot, \cdot \rangle$, and operators are defined on dense domains $\mathcal{D} \subset \mathcal{H}$ such that closure and self-adjoint extensions exist where required. All physically relevant operators are assumed to admit self-adjoint or essentially self-adjoint extensions on the specified domain. This anchors the subsequent operator constructions and symplectic formalism in a well-defined functional analytic setting.

2.1. Matter Sector: Wavefunction Hilbert Space

We begin with the standard Hilbert space for a single-particle (or effective single-particle) matter wavefunction,

$$\mathcal{H}_\psi = L^2\left(\mathbb{R}^3\right) = \left\{\psi : \mathbb{R}^3 \to \mathbb{C} \,|\, \int |\psi(\boldsymbol{x})|^2 \, \mathrm{d}^3x < \infty\right\}. \tag{6}$$

The inner product is the usual

$$\langle \psi_1 | \psi_2 \rangle = \int_{\mathbb{R}^3} \psi_1^*(\boldsymbol{x}) \psi_2(\boldsymbol{x}) \mathrm{d}^3x. \tag{7}$$

The matter-sector Hamiltonian is written as

$$H_\psi = -\frac{\hbar^2}{2m}\nabla^2 + U(\boldsymbol{x}), \tag{8}$$

where m is the bare matter mass parameter and $U(\boldsymbol{x})$ a possible external potential. At this stage U plays no dynamical role; its purpose is to allow comparison with the usual Schrödinger picture [7]. All nontrivial interaction with the timeon field will enter through a separate interaction Hamiltonian.

2.2. Timeon Sector: Field Configuration Space

The timeon field is a complex scalar function,

$$\Phi(\boldsymbol{x}) = \hat{t}(\boldsymbol{x}) \mathrm{e}^{i\theta(\boldsymbol{x})}, \tag{9}$$

with amplitude $\hat{t} \geq 0$ encoding local time density and phase θ encoding an internal $U(1)$ degree of freedom. Before introducing dynamics (which will come in Section 3), we specify the kinematic Hilbert space $\mathcal{H}_\Phi$ as the space of square-integrable wavefunctionals over field configurations:

$$\mathcal{H}_\Phi = L^2\left(\mathcal{C}_\Phi, \mathcal{D}\Phi\right), \tag{10}$$

where $\mathcal{C}_\Phi$ is the configuration space of complex fields and $\mathcal{D}\Phi$ is the formal functional measure. A generic state in this sector is written

$$\Psi_\Phi\left[\Phi(\cdot)\right], \tag{11}$$

a functional of the spatial profile of the timeon field. For classical field configurations, expectation values will later be dominated by stationary-phase contributions corresponding to finite-energy configurations of Φ. The timeon-sector Hamiltonian will be developed fully in Section 3. For now, we denote it symbolically by

$$H_\Phi\left[\Phi, -i\hbar\delta/\delta\Phi\right], \tag{12}$$

emphasizing that it acts on functionals of the field.

2.3. Composite Hilbert Space

The system consisting of matter and timeon field is described on the tensor-product Hilbert space [8]

$$\mathcal{H} = \mathcal{H}_{\psi} \otimes \mathcal{H}_{\Phi}. \tag{13}$$

A general state has the form

$$\Psi(\boldsymbol{x}, \Phi) = \psi(\boldsymbol{x}) \otimes \Psi_{\Phi}[\Phi] + \sum_i c_i \psi_i(\boldsymbol{x}) \otimes \Psi_{\Phi,i}[\Phi] + \cdots, \tag{14}$$

but for physical baryons we will be concerned with states that are approximately separable into a localised matter wavefunction and a localised timeon configuration. The inner product on $\mathcal{H}$ factorizes:

$$\langle \Psi_1 | \Psi_2 \rangle = \langle \psi_1 | \psi_2 \rangle_{\psi} \langle \Psi_{\Phi,1} | \Psi_{\Phi,2} \rangle_{\Phi}. \tag{15}$$

2.4. Composite Hamiltonian

The dynamics of the joint system are governed by a Hamiltonian of the form

$$H = H_{\psi} \otimes \mathbb{I}_{\Phi} + \mathbb{I}_{\psi} \otimes H_{\Phi} + H_{\text{int}}, \tag{16}$$

where:

- H_{ψ} acts only on the matter wavefunction,
- H_{Φ} acts only on the timeon sector, and
- H_{int} couples them locally.

To anticipate later developments, the interaction Hamiltonian will take the form

$$H_{\text{int}} = g \int \mathrm{d}^3 x \, |\psi(\boldsymbol{x})|^2 \, |\Phi(\boldsymbol{x})|^2, \tag{17}$$

where g is a coupling constant. This term expresses the intuitive fact that high matter probability density—and, over aeon timescales, chrono-emergent tunnelling—tends to drive the timeon field into high-amplitude, highly stable atomic configurations. Likewise, a region in which the timeon field has adopted the atomic phase produces an effective potential for the matter wavefunction. In classical field realizations, the operator $|\Phi|^2$ becomes simply the squared amplitude $\hat{t}^2(\boldsymbol{x})$; when quantised, it acts as a local operator multiplying the wavefunctional Ψ_{Φ}.

2.5. Definition of the Baryon Partner State

We now define the key object of the theory: the *Baryon Partner State* (BPS). A BPS is a joint eigenstate of the composite Hamiltonian (16) of the form

$$\Psi_{\text{BPS}} = \psi_{\text{BPS}}(\boldsymbol{x}) \otimes \Psi_{\Phi,\text{BPS}}[\Phi], \tag{18}$$

such that

$$H \Psi_{\text{BPS}} = E_{\text{BPS}} \Psi_{\text{BPS}}. \tag{19}$$

The eigenvalue E_{BPS} defines the effective mass of the composite object,

$$m_{\mathrm{BPS}} = \frac{E_{\mathrm{BPS}}}{c^2}, \tag{20}$$

and the structure of $\Psi_{\Phi,\mathrm{BPS}}$ determines the internal charge and stability properties. The BPS must satisfy three physical conditions:

1) **Finite energy:** the timeon configuration must minimise H_Φ subject to boundary conditions (derived in Section 4).

2) **Self-consistency:** the matter wavefunction ψ_{BPS} must be bound to the highly stable timeon configuration that it helps generate.

3) **Locality:** both ψ_{BPS} and $\Psi_{\Phi,\mathrm{BPS}}$ must be spatially localised, yielding a finite, well-defined composite excitation.

These conditions distinguish BPS configurations from arbitrary fluctuations of either field sector. Only when the interaction term (17) is included do localised atomic-phase solutions of the timeon field become highly stable, and only then does the matter wavefunction acquire a localised baryonic structure.

2.6. Remarks on Separability and Entanglement

While the idealized definition above uses a separable tensor product state $\psi \otimes \Psi_\Phi$, the physical BPS is generally entangled. The presence of the interaction Hamiltonian implies that the true ground-state solution takes the form

$$\Psi_{\mathrm{BPS}}(\boldsymbol{x}, \Phi) = \sum_i c_i \psi_i(\boldsymbol{x}) \otimes \Psi_{\Phi,i}[\Phi], \tag{21}$$

with coefficients c_i determined by minimizing the total energy functional. The separable form is therefore best understood as the leading-order description in a Born-Oppenheimer-like approximation [9] in which the timeon field provides a slowly varying background for the matter wavefunction. This structure will be made explicit in later sections, where we derive both the static timeon configurations and the coupled evolution equations for ψ and Φ.

3. Timeon Field Theory: Lagrangian, Hamiltonian, and Phase Structure

We now construct the timeon field theory that governs the time-density field introduced in the previous section. The timeon is treated as a complex scalar field,

$$\Phi(x) = \hat{t}(x) \mathrm{e}^{i\theta(x)}, \tag{22}$$

with amplitude $\hat{t} \geq 0$ capturing local time density and phase θ carrying an internal $U(1)$ structure. Throughout we use the four-vector notation $x^\mu = (ct, \boldsymbol{x})$ and the metric signature $(+,-,-,-)$. The framework developed here is not derived via canonical quantisation of a classical precursor, but instead defines quantum structure intrinsically through the algebra of the timeon field and its coupling to the matter sector. The goal of this section is to build the complete field-theoretic framework: the Lagrangian density, Euler-Lagrange equations, Hamiltonian density, and the potential structure that supports vacuum and

atomic phases.

3.1. Lagrangian Density

We adopt a physical Lagrangian density scaled by a stiffness modulus Z_t (units of Force) to ensure the scalar field yields units of Energy Density:

$$\mathcal{L}_\Phi = \frac{Z_t}{2}\left[\left(\partial_\mu \hat{t}\right)^2 + \hat{t}^2\left(\partial_\mu \theta\right)^2\right] - V\left(\hat{t}^2\right). \tag{23}$$

Here, the amplitude field $\hat{t}$ has units of time-density (s/m) and Z_t provides the necessary conversion to Joules/m^3.

The two degrees of freedom are thus:

- $\hat{t}$: a real amplitude field controlling time-density,
- θ : a Goldstone-like phase variable.

We will see that stable baryonic configurations arise primarily from nonlinear structure in V and localised gradients in $\hat{t}$.

3.2. Euler-Lagrange Equations

The Euler-Lagrange equation for the complex field is:

$$\partial_\mu\left(\frac{\partial \mathcal{L}_\Phi}{\partial\left(\partial_\mu \Phi^*\right)}\right) - \frac{\partial \mathcal{L}_\Phi}{\partial \Phi^*} = 0. \tag{24}$$

Working directly with Φ yields the d'Alembertian dynamics [7]:

$$\Box\Phi + \frac{\partial V}{\partial \Phi^*} = 0, \tag{25}$$

where $\Box = \partial_\mu \partial^\mu$ is the d'Alembertian. Alternatively, in amplitude/phase variables:

Amplitude equation:

$$\Box\hat{t} - \hat{t}\left(\partial_\mu \theta\right)^2 + V'\left(\hat{t}^2\right)\hat{t} = 0, \tag{26}$$

Phase equation:

$$\partial_\mu\left(\hat{t}^2 \partial^\mu \theta\right) = 0. \tag{27}$$

where V' denotes derivative with respect to its argument $\left(\hat{t}^2\right)$. The phase equation expresses the local conservation of a $U(1)$ -like current,

$$j^\mu = 2\hat{t}^2 \partial^\mu \theta, \tag{28}$$

which is the Noether current [10] that will play a role in defining effective "charge" of BPS solutions.

3.3. Hamiltonian Density

To compute energies of static configurations (including BPS cores) we require the Hamiltonian density. For a complex scalar,

$$\mathcal{H}_\Phi = \left|\pi_\Phi\right|^2 + \left|\nabla\Phi\right|^2 + V\left(\left|\Phi\right|^2\right), \tag{29}$$

where the canonical momentum is

$$\pi_{\Phi} = \frac{\partial \mathcal{L}_{\Phi}}{\partial\left(\partial_t \Phi^*\right)} = \dot{\Phi}. \tag{30}$$

Thus explicitly,

$$\mathcal{H}_{\Phi} = \left|\dot{\Phi}\right|^2 + \left|\nabla\Phi\right|^2 + V\left(\left|\Phi\right|^2\right). \tag{31}$$

In polar form:

$$\left|\nabla\Phi\right|^2 = \left(\nabla\hat{t}\right)^2 + \hat{t}^2\left(\nabla\theta\right)^2, \tag{32}$$

and

$$\left|\dot{\Phi}\right|^2 = \dot{\hat{t}}^2 + \hat{t}^2\dot{\theta}^2. \tag{33}$$

For static solutions (all BPS cores considered here), $\dot{\hat{t}} = 0$ and $\dot{\theta} = 0$, yielding the static Hamiltonian density:

$$\boxed{\mathcal{H}_{\Phi}^{\text{static}} = \left(\nabla\hat{t}\right)^2 + \hat{t}^2\left(\nabla\theta\right)^2 + V\left(\hat{t}^2\right).} \tag{34}$$

This is the expression we will minimise to obtain baryonic solutions.

3.4. Double-Well Potential and Phase Structure

To support localised, highly stable atomic-phase reconfigurations, the potential must have at least two distinct minima:

$$V\left(\hat{t}^2\right) = \lambda\left(\hat{t}^2 - v_{\text{vac}}^2\right)^2\left(\hat{t}^2 - v_{\text{atom}}^2\right)^2, \tag{35}$$

with $v_{\text{atom}} > v_{\text{vac}} \geq 0$. The minima occur at $\hat{t} = v_{\text{vac}}$ and $\hat{t} = v_{\text{atom}}$. We refer to these as:

- **Vacuum phase:** $\hat{t} = v_{\text{vac}}$ (low time density)
- **Atomic phase:** $\hat{t} = v_{\text{atom}}$ (Condensed Lattice Phase)

The barrier separating them determines tunnelling rates and the nucleation structure of atomic-phase reconfigurations (**Figure 1**).

Quadratic expansion and mass scales

Expanding around each minimum yields the small-oscillation mass:

- Around vacuum phase:

$$\hat{t}\left(x\right) = v_{\text{vac}} + \delta\hat{t}\left(x\right), \tag{36}$$

$$m_{\text{vac}}^2 = \left.\frac{\mathrm{d}^2 V}{\mathrm{d}\hat{t}^2}\right|_{\hat{t}=v_{\text{vac}}}. \tag{37}$$

- Around atomic phase:

$$\hat{t}\left(x\right) = v_{\text{atom}} + \delta\hat{t}\left(x\right), \tag{38}$$

$$m_{\text{atom}}^2 = \left.\frac{\mathrm{d}^2 V}{\mathrm{d}\hat{t}^2}\right|_{\hat{t}=v_{\text{atom}}}. \tag{39}$$

Both masses will appear later in the fluctuation spectrum of BPS cores.

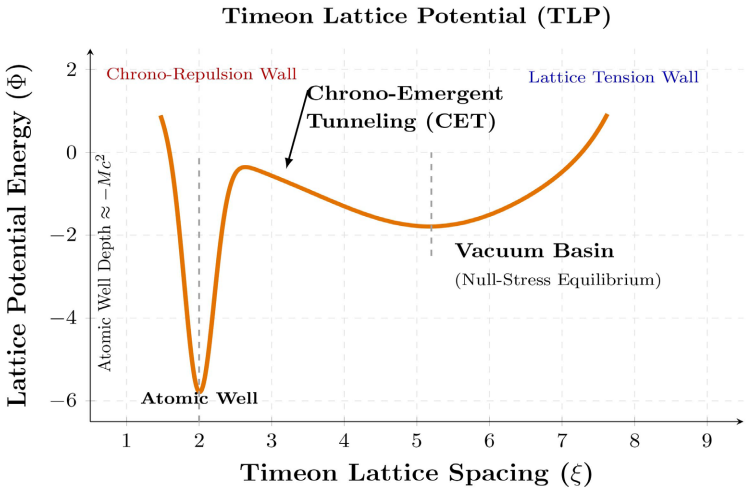

Figure 1. The Timeon Lattice Potential (TLP). The potential energy density $V(\hat{t})$ features a metastable Vacuum basin and a stable Atomic well. Baryon Partner State formation corresponds to tunnelling through the barrier separating these phases. **Scope of this plot:** This theoretical landscape is restricted to the formation of discrete Baryon Partner States and intentionally *excludes* black hole interiors and chrono-shear events (*i.e.*, dense- and shear-time-density phases).

3.5. Energetics of Phase Boundaries

Finite-energy static solutions require that $\hat{t}$ interpolate between different minima over a finite spatial width. The energy per unit area of such an interface ("domain wall") is

$$\sigma = \int_{v_{\text{vac}}}^{v_{\text{atom}}} \mathrm{d}\hat{t}\sqrt{2V\left(\hat{t}^2\right)}. \tag{40}$$

This quantity plays a central role in critical-radius calculations, atomic-phase nucleation barriers, and BPS core stability. We will use σ in Section 4 and Section 5 to derive baryon mass and tunnelling thresholds.

3.6. Summary of Key Results from Section 3

- The timeon field is governed by the Lagrangian (23) and Hamiltonian density (34).
- The potential must have at least two minima, leading to vacuum and atomic phases.
- Domain walls have finite surface tension σ given by (40).
- The small-oscillation masses in each phase determine the reconfiguration spectrum of baryons.

The next section constructs explicit finite-energy static solutions representing Baryon Partner States.

4. Static Baryon Partner State (BPS) Solutions

We now derive the finite-energy, static configurations of the timeon field that cor-

respond to Baryon Partner States (BPS). These solutions represent localised regions of atomic phase embedded within the vacuum phase, stabilised by the nonlinear structure of the potential and, later (Section 6), by coupling to the matter wavefunction. The goal of this section is to obtain the radial profile of a static BPS, its energy, and its effective charge, and to establish the topological reasons why such configurations cannot decompose into smaller constituents.

4.1. Spherical Ansatz

Because baryons are experimentally observed to be approximately spherically symmetric in their lowest-energy state, we impose spherical symmetry on the static timeon configuration:

$$\Phi(\boldsymbol{x}) = \hat{t}(r)\mathrm{e}^{i\theta(r)}, \tag{41}$$

where $r = |\boldsymbol{x}|$. Staticity implies $\partial_t \hat{t} = 0$ and $\partial_t \theta = 0$. Thus only spatial gradients contribute to the energy. Under spherical symmetry:

$$|\nabla\Phi|^2 = (\partial_r \hat{t})^2 + \hat{t}^2 (\partial_r \theta)^2. \tag{42}$$

The static energy functional from (34) becomes:

$$E[\hat{t},\theta] = 4\pi\int_0^\infty r^2 \left[(\hat{t}')^2 + \hat{t}^2 (\theta')^2 + V(\hat{t}^2) \right] \mathrm{d}r, \tag{43}$$

where primes denote derivatives with respect to r.

4.2. Boundary Conditions

Finite-energy solutions require:

1) **Core condition:** The field must approach the atomic phase at $r = 0$,

$$\hat{t}(0) = v_{\text{atom}}, \quad \theta'(0) = 0.$$

2) **Vacuum exterior:** At large r the field returns to vacuum phase equilibrium:

$$\hat{t}(r \to \infty) = v_{\text{vac}}.$$

3) **Finite energy:** The phase gradient must vanish outside the core,

$$\theta'(r \to \infty) = 0.$$

4) **Regularity at $r = 0$:** Terms like r^{-2} must not diverge, implying

$$\hat{t}'(0) = 0, \quad \theta(0) = \text{finite}.$$

These conditions uniquely determine the qualitative shape of a BPS profile.

4.3. Radial Field Equations

Variation of the energy functional (43) yields the coupled radial Euler-Lagrange equations [7].

Amplitude equation:

$$\hat{t}'' + \frac{2}{r}\hat{t}' - \hat{t}(\theta')^2 - \frac{1}{2}V'(\hat{t}^2)(2\hat{t}) = 0, \tag{44}$$

Phase equation:

$$\frac{\mathrm{d}}{\mathrm{d}r}\left(r^2\hat{t}^2\theta'\right)=0. \tag{45}$$

Integrating the phase equation:

$$r^2\hat{t}^2\theta'=Q, \tag{46}$$

where Q is a constant of integration. This constant behaves as a conserved **topological charge** associated with phase gradients in the timeon field. Thus:

$$\theta'(r)=\frac{Q}{r^2\hat{t}(r)^2}. \tag{47}$$

Substituting back into (44) yields the single radial equation:

$$\hat{t}''+\frac{2}{r}\hat{t}'-\frac{Q^2}{r^4\hat{t}^3}-V'\left(\hat{t}^2\right)\hat{t}=0. \tag{48}$$

This nonlinear ODE defines the full static BPS profile.

4.4. Interpretation of the Charge Parameter Q

The quantity Q controls the strength of the phase gradient in the core region. Several key properties follow:

- If $Q=0$, the phase is constant and the solution has no internal $U(1)$ excitation. This describes a neutral baryonic configuration (the analogue of the neutron, if the $U(1)$ charge is identified with electric charge).
- If $Q\neq 0$, the core hosts a localised winding of the phase, contributing to a finite $U(1)$ charge density:

$$j^r=\hat{t}^2\theta'.$$

- Because the energy density contains

$$\hat{t}^2\left(\theta'\right)^2=\frac{Q^2}{r^4\hat{t}^2},$$

the charge is confined to regions where $\hat{t}$ is large (atomic phase). This provides a direct algebraic mechanism for baryonic charge confinement.

Clarification of the simultaneous roles of Q. The quantity Q plays multiple roles simultaneously, and we clarify each:

1) **Q as an integration constant.** Equation (46) arises by integrating the radial phase equation $\frac{\mathrm{d}}{\mathrm{d}r}\left(r^2\hat{t}^2\theta'\right)=0$. In the static, spherically symmetric setting of Section, Q is therefore first and foremost a *constant of integration* that parameterises the family of solutions. Different values of Q give physically distinct configurations.

2) **Q as a Noether charge.** The phase equation itself expresses local conservation of the $U(1)$ Noether current $j^\mu=2\hat{t}^2\partial^\mu\theta$ (derived in **Appendix C**). The static radial quantity Q measures the total radial phase-current threading each spherical shell, and by the phase equation this is the same on every shell—hence a

constant.

3) ***Q* as a topological winding invariant.** Unwinding the phase from $Q \neq 0$ to $Q = 0$ requires passing through a configuration in which $\hat{t} = 0$ at some radius, which carries infinite energy from the charge-confinement term $Q^2/\left(r^4\hat{t}^2\right)$ in the energy functional. Q is therefore also a *topological invariant* of the BPS.

Summary. Q is simultaneously an integration constant (in the ODE sense), a conserved Noether charge (from the global $U(1)$ symmetry), and a topological winding invariant (from the energetic barrier against phase unwinding). The integer character of Q for physical BPS states follows from requiring that $e^{i\theta}$ be single-valued on each spherical shell, yielding $Q \in \mathbb{Z}$ and thus charge quantisation. The phrase "conserved charge" in the Introduction and the phrase "integration constant" in the present section refer to the same quantity viewed at different levels of description.

4.5. Energy of a BPS Configuration

Substituting (47) into the static energy functional yields:

$$E_{\mathrm{BPS}} = 4\pi\int_0^\infty r^2\left[\left(\hat{t}'\right)^2 + \frac{Q^2}{r^4\hat{t}^2} + V\left(\hat{t}^2\right)\right]\mathrm{d}r. \tag{49}$$

Three competing contributions determine the radius and stability of a BPS:

1) **Gradient energy:** favours slowly varying $\hat{t}$.

2) **Phase-gradient energy (charge term):** grows rapidly as $\hat{t} \to 0$, confining charge to the atomic-phase core. Note that Q here denotes the timeon $U(1)$ Noether charge; its identification with electric charge in units of e is the subject of forthcoming work.

3) **Potential energy:** favours either vacuum or atomic phase in bulk.

Balancing these terms yields a stable finite-radius atomic-phase core.

4.6. Thin-Wall Approximation

When the energy barrier between vacuum and atomic phase is large relative to gradient contributions, the BPS resembles a domain-wall configuration of radius R. In this regime we approximate:

$$\hat{t}(r) \approx \begin{cases} v_{\mathrm{atom}}, & r < R \\ v_{\mathrm{vac}}, & r > R \end{cases} \quad \text{with a narrow transition of width } \delta \ll R.$$

The energy simplifies to:

$$E_{\mathrm{BPS}}(R) = 4\pi R^2\sigma + \frac{4\pi Q^2}{v_{\mathrm{atom}}^2 R} + \frac{4\pi}{3}R^3\Delta V, \tag{50}$$

where $\Delta V = V\left(v_{\mathrm{atom}}^2\right) - V\left(v_{\mathrm{vac}}^2\right) < 0$. Minimizing (50) gives the equilibrium BPS radius:

$$\frac{\mathrm{d}E}{\mathrm{d}R} = 0 \;\Rightarrow\; 8\pi R\sigma - \frac{4\pi Q^2}{v_{\mathrm{atom}}^2 R^2} + 4\pi R^2\Delta V = 0. \tag{51}$$

This cubic equation determines the physical radius as a function of charge Q,

potential parameters, and surface tension.

Mass estimate from the thin-wall formula. Setting $Q=0$ for simplicity (charge-free limit), minimizing $E(R)=4\pi R^2\sigma+\frac{4\pi}{3}R^3\Delta V$ gives the critical radius

$$R_*=-\frac{2\sigma}{\Delta V}=\frac{2\sigma}{|\Delta V|}, \tag{52}$$

and the corresponding BPS mass

$$M_{\mathrm{BPS}}=\frac{16\pi}{3}\frac{\sigma^3}{|\Delta V|^2}. \tag{53}$$

Here σ (energy per unit area) and $|\Delta V|$ (energy per unit volume difference between phases) are the two free parameters of the thin-wall approximation. For $R_*\sim 1\,\mathrm{fm}$ (proton charge radius) and $M_{\mathrm{BPS}}\sim 938\ \mathrm{MeV}$ (proton mass), dimensional analysis requires $\sigma\sim(200\ \mathrm{MeV})^3$ and $|\Delta V|\sim(200\ \mathrm{MeV})^4$, coinciding with the QCD confinement scale $\Lambda_{\mathrm{QCD}}\approx 200\ \mathrm{MeV}$. This numerical coincidence is encouraging, though a full parameter fit to the light baryon spectrum—including isospin breaking and coupling-to-matter corrections—is deferred to a forthcoming companion paper.

4.7. Topological Stability and Confinement

The BPS core is topologically protected by the structure of the phase variable θ and by the requirement that $\hat{t}$ remain nonzero inside the atomic region. Key features:

- The phase equation mandates that $r^2\hat{t}^2\theta'=Q$. If one attempted to split a BPS into smaller charged fragments, this relation would require singularities (where $\hat{t}=0$) to maintain total Q. Such configurations have infinite energy.
- The volume energy density difference $\Delta V<0$ favours a stable core of atomic phase.
- The gradient term penalises fragmentation because multiple small atomic-phase regions have larger total surface area than a single region of the same volume.

Thus the BPS is intrinsically confined: it cannot decompose without energy divergence or violation of charge conservation.

4.8. Summary of Section 4

We have:

- Written the full radial equations for static timeon configurations.
- Identified the conserved charge Q associated with phase gradients.
- Derived the energy functional for BPS solutions.
- Obtained approximate analytic behaviour via the thin-wall limit.
- Shown that confinement follows directly from the algebraic and topological structure of the timeon field.

These results prepare the ground for computing tunnelling, atomic-phase nucleation, and BPS nucleation in the next section.

5. Vacuum-to-Atomic Tunnelling and Bubble Nucleation of Atomic-Phase Reconfigurations

In the previous section we constructed static Baryon Partner State configurations by minimizing the energy functional. We now consider the opposite question: *How does a localised region of atomic phase form dynamically within the vacuum*? The answer requires a tunnelling calculation in which the timeon field transitions from the vacuum minimum to the atomic minimum through a Euclidean "bounce" solution. This section develops the complete quantum tunnelling formalism for the timeon field, derives the critical radius for atomic-phase nucleation, and identifies the tunnelling exponent governing BPS formation.

5.1. Euclidean Action for the Timeon Field

Quantum tunnelling in scalar field theory is governed by the Euclidean action, obtained by Wick rotation $t \to -i\tau$ [11]:

$$S_E[\Phi] = \int \mathrm{d}\tau \mathrm{d}^3x \left[\left|\partial_\tau \Phi\right|^2 + \left|\nabla\Phi\right|^2 + V\left(\left|\Phi\right|^2\right) \right]. \tag{54}$$

For tunnelling from the vacuum to the atomic phase, the relevant solutions possess $O(4)$ symmetry in the Euclidean coordinates

$$\rho^2 = \tau^2 + r^2, \tag{55}$$

leading to the ansatz

$$\Phi(\rho) = \hat{t}(\rho)\mathrm{e}^{i\theta(\rho)}. \tag{56}$$

The Euclidean action becomes

$$S_E\left[\hat{t},\theta\right] = 2\pi^2 \int_0^\infty \rho^3 \left[\left(\hat{t}'\right)^2 + \hat{t}^2 \left(\theta'\right)^2 + V\left(\hat{t}^2\right) \right] \mathrm{d}\rho. \tag{57}$$

5.2. Euclidean Field Equations

The Euler-Lagrange equations corresponding to (57) are:

Amplitude:

$$\hat{t}'' + \frac{3}{\rho}\hat{t}' - \hat{t}\left(\theta'\right)^2 - V'\left(\hat{t}^2\right)\hat{t} = 0. \tag{58}$$

Phase:

$$\frac{\mathrm{d}}{\mathrm{d}\rho}\left(\rho^3 \hat{t}^2 \theta'\right) = 0. \tag{59}$$

Integrating:

$$\rho^3 \hat{t}^2 \theta' = Q_E, \tag{60}$$

where Q_E is a Euclidean analogue of the charge parameter. Most tunnelling cal-

culations assume $Q_E = 0$, corresponding to a phase-uniform bounce. We will treat this case first, then include nonzero charge.

5.3. Bounce Solution for $Q_E = 0$

With $\theta' = 0$, the Euclidean equation reduces to:

$$\hat{t}'' + \frac{3}{\rho}\hat{t}' - V'\left(\hat{t}^2\right)\hat{t} = 0. \tag{61}$$

Boundary conditions:

$$\hat{t}'(0) = 0, \tag{62}$$

$$\hat{t}\left(\rho \to \infty\right) = v_{\text{vac}}. \tag{63}$$

The solution interpolates from the atomic minimum near $\rho = 0$ to the vacuum minimum as $\rho \to \infty$. The configuration is called the *bounce* and denoted $\hat{t}_B(\rho)$ [12]. The tunnelling exponent is:

$$B = S_E\left[\hat{t}_B\right] - S_E\left[\hat{t}_{\text{vac}}\right]. \tag{64}$$

The nucleation rate per unit volume is:

$$\Gamma/V \sim A\mathrm{e}^{-B/\hbar}, \tag{65}$$

where A is a fluctuation determinant prefactor.

5.4. Thin-Wall Limit and Critical Bubble Radius

When the barrier separating the two minima is large compared to their energy difference, the bounce resembles a thin-walled atomic-phase domain. In this limit, the Euclidean action reduces to:

$$S_E(R) = 2\pi^2 R^3 \sigma - \frac{\pi^2}{2} R^4 \Delta V, \tag{66}$$

where:

- σ is the surface tension from (40),
- $\Delta V = V\left(v_{\text{atom}}^2\right) - V\left(v_{\text{vac}}^2\right) < 0$.

Differentiating:

$$\frac{\mathrm{d}S_E}{\mathrm{d}R} = 6\pi^2 R^2 \sigma - 2\pi^2 R^3 \Delta V = 0, \tag{67}$$

leading to the **critical radius**:

$$R_c = \frac{3\sigma}{|\Delta V|}. \tag{68}$$

Only atomic-phase domains with $R \geq R_c$ expand; smaller domains collapse. Substituting back:

$$B_{\text{thin}} = \frac{27\pi^2 \sigma^4}{2|\Delta V|^3}. \tag{69}$$

This closed-form expression is crucial to estimating BPS nucleation probabilities.

5.5. Effect of Nonzero Charge Q_E

If $Q_E \neq 0$, the Euclidean phase gradient contributes a centrifugal-like term:

$$\hat{t}^2 (\theta')^2 = \frac{Q_E^2}{\rho^6 \hat{t}^2}. \tag{70}$$

This term:

- suppresses configurations where $\hat{t}$ is small,
- drives the interior of the atomic-phase domain toward the atomic phase,
- increases the effective surface pressure,
- decreases the tunnelling exponent B.

The corrected thin-wall action becomes:

$$S_E(R) = 2\pi^2 R^3 \sigma - \frac{\pi^2}{2} R^4 \Delta V + \frac{C Q_E^2}{R^2 v_{\text{atom}}^2}, \tag{71}$$

where C is an order-one geometric constant. Minimizing yields a modified critical radius:

$$R_c(Q_E) \approx \left(\frac{3\sigma}{|\Delta V|} + \frac{Q_E^2}{3\pi^2 v_{\text{atom}}^2 \sigma} \right) + \mathcal{O}\left(Q_E^4\right). \tag{72}$$

Thus:

- charge slightly expands the critical radius,
- but makes the atomic phase more energetically favoured inside the atomic-phase domain,
- and typically decreases the tunnelling exponent.

Charged tunnelling therefore increases the likelihood of BPS formation, as does the progression of aeon timescales.

5.6. Interpretation: Matter Formation via Timeon Tunneling

A physically transparent interpretation emerges:

1) The vacuum phase is metastable, adjacent to a more highly stable atomic-phase configuration accessible via probabilistic tunnelling.

2) Quantum fluctuations—and, over aeon timescales, chrono-emergent tunnelling—occasionally nucleate a small region of atomic phase.

3) If the region exceeds the critical radius R_c, it expands.

4) The presence of matter (Section 6) reduces R_c locally by compressing the timeon field.

5) The expanding atomic region forms the core of a BPS.

Thus baryon formation is not simply imposed—it is a dynamical outcome of timeon-field tunnelling stabilised by matter-wave coupling.

5.7. Summary of Section 5

We have:

- Formulated vacuum-to-atomic tunnelling using the Euclidean action.
- Derived the bounce equations and boundary conditions.
- Obtained the critical radius R_c and tunnelling exponent B.
- Extended the thin-wall approximation to include charge.
- Established the mechanism by which atomic-phase reconfigurations become stabilised baryonic cores.

The next section introduces the coupling to the matter wavefunction, completing the dynamical picture of Baryon Partner States.

6. Coupling to the Matter Wavefunction and Self-Consistent Dynamics

Up to this point, the timeon field has been treated independently of the matter wavefunction. We now introduce the essential ingredient of the theory: a local interaction between the matter density $|\psi|^2$ and the timeon amplitude $\hat{t}^2$. This coupling allows high matter density $|\psi|^2$ to drive the timeon field toward the atomic phase, since regions of large $|\psi|^2$ effectively lower the local potential barrier for the timeon amplitude $\hat{t}$, favouring the atomic minimum and stabilising Baryon Partner States (BPS). Conversely, the timeon configuration modifies the effective potential seen by the matter wavefunction, binding ψ to the atomic core it helps generate. The result is a fully self-consistent system where matter and timeon fields mutually determine each other's configuration.

Dynamical Regime and Justification of the Coupled System

The matter wavefunction $\psi(\mathbf{x},t)$ in this section is treated as nonrelativistic, governed by the Schrödinger equation. The timeon field $\Phi = \hat{t}\mathrm{e}^{i\theta}$ is a relativistic scalar field obeying the d'Alembertian equation of motion. This asymmetric treatment is deliberate and internally consistent for the following reasons.

1) **Separation of scales.** The BPS is a composite object in which the timeon field provides a slowly varying, spatially extended background and the matter wavefunction describes a single quantum particle localised within that background. This is precisely the regime of validity of the Born-Oppenheimer approximation [9]: the "heavy" sector (timeon field, with large gradient energy and slow internal dynamics) and the "light" sector (matter particle, with fast quantum oscillations at fixed timeon background) are treated on separate footings.

2) **Nonrelativistic matter approximation.** The matter particle is taken to be nonrelativistic ($v \ll c$, or equivalently $E_\psi \ll mc^2$). In this regime the Dirac equation and Klein-Gordon equation both reduce to the Schrödinger equation [7], so the use of $i\hbar\partial_t\psi = H_\psi\psi$ is the correct leading-order description within the nonrelativistic sector. Relativistic corrections to the matter sector are of order $(v/c)^2$ and are suppressed.

3) **Frame choice.** All equations in this section are written in the rest frame of the BPS centre of mass. In this frame the static timeon profile $\hat{t}_0(r)$ is time-independent, and the matter wavefunction $\psi(r)$ satisfies a time-independent eigenvalue problem. Lorentz-boosted frames are discussed in Section 8 via the col-

lective-coordinate approach.

4) **Limits of validity.** The coupled system is valid when: (1) the matter particle's kinetic energy satisfies $\hbar^2 |\nabla\psi|^2 / (2m) \ll mc^2$; (2) the timeon field varies on length scales large compared to the de Broglie wavelength of the matter particle; and (3) the coupling g is small enough that back-reaction of $|\psi|^2$ on the timeon profile can be treated perturbatively in the first iteration, before full self-consistency is imposed by iteration. Violations of condition (1) would require replacing the Schrödinger equation with the Klein-Gordon or Dirac equation for the matter sector. Violations of conditions (2) or (3) would require numerical self-consistent treatment without a Born-Oppenheimer separation. Both extensions are planned for future work.

5) **Consistency.** There is no fundamental inconsistency in coupling a nonrelativistic quantum particle to a relativistic field. This is standard practice in condensed-matter physics (electrons in a phonon field), nuclear physics (nucleons in a pion field), and atomic physics (atoms in the electromagnetic field treated in the nonrelativistic limit). The timeon-matter system falls into the same category.

6.1. Interaction Hamiltonian

We postulate the simplest local, scalar, bilinear interaction:

$$H_{\text{int}} = g \int \mathrm{d}^3x \left|\psi(\boldsymbol{x},t)\right|^2 \left|\Phi(\boldsymbol{x},t)\right|^2, \tag{73}$$

where g is a real coupling constant controlling the strength of the compression effect. Writing $\Phi = \hat{t}\,\mathrm{e}^{i\theta}$:

$$|\Phi|^2 = \hat{t}^2.$$

Thus the interaction term becomes:

$$H_{\text{int}} = g \int \mathrm{d}^3x |\psi|^2 \hat{t}^2. \tag{74}$$

This is the lowest-order operator capable of:

- lowering the effective potential seen by $\hat{t}$ in regions where $|\psi|^2$ is large,
- raising the effective potential of ψ in regions where $\hat{t}$ is small,
- and creating a self-localizing composite eigenstate.

The interaction is local, Hermitian, and preserves all global symmetries.

6.2. Total Hamiltonian and Equations of Motion

The full Hamiltonian is:

$$H = H_\psi + H_\Phi + H_{\text{int}}, \tag{75}$$

with H_ψ and H_Φ defined in earlier sections. We now derive the equations governing the coupled dynamics.

6.2.1. Matter Wavefunction Equation

Varying the total action with respect to ψ^* yields:

$$i\hbar \frac{\partial\psi}{\partial t} = \left[-\frac{\hbar^2}{2m}\nabla^2 + U(\boldsymbol{x}) + g\hat{t}^2(\boldsymbol{x},t) \right]\psi. \tag{76}$$

Thus the timeon amplitude $\hat{t}^2$ contributes an effective potential:

$$U_{\text{eff}}(\boldsymbol{x}) = U(\boldsymbol{x}) + g\hat{t}^2(\boldsymbol{x}). \tag{77}$$

Regions of high $\hat{t}$ (atomic phase) attract the matter wavefunction, creating a stable bound state. This is the coupled Schrödinger equation [7].

6.2.2. Timeon Amplitude Equation

Varying the total action with respect to $\hat{t}$ yields:

$$\Box\hat{t} - \hat{t}\left(\partial_\mu\theta\right)^2 + V'\left(\hat{t}^2\right)\hat{t} = -g|\psi|^2\hat{t}. \tag{78}$$

The right-hand side shows explicitly:

- matter density suppresses the vacuum minimum,
- and deepens the atomic minimum,
- effectively tilting the potential energy in favor of the atomic phase.

More precisely, the interaction modifies the potential:

$$V_{\text{eff}}\left(\hat{t}^2\right) = V\left(\hat{t}^2\right) + g|\psi|^2\hat{t}^2.$$

Thus:

- if $g > 0$: matter pushes the timeon field to larger amplitudes (atomic phase),
- if $g < 0$: matter repels the atomic phase (we focus on $g > 0$).

6.2.3. Timeon Phase Equation

Variation with respect to θ yields the modified current conservation equation:

$$\partial_\mu\left(\hat{t}^2\partial^\mu\theta\right) = 0. \tag{79}$$

Because H_{int} depends only on $\hat{t}^2$, the $U(1)$ phase remains a conserved degree of freedom. The associated charge Q remains valid in the presence of matter.

6.3. Self-Consistent BPS Equations

Since a static BPS is time-independent, we set $\partial_t = 0$. The coupled static system is:

$$-\frac{\hbar^2}{2m}\nabla^2\psi + \left[U(\boldsymbol{x}) + g\hat{t}^2(\boldsymbol{x})\right]\psi = E_\psi\psi, \tag{80}$$

$$\nabla^2\hat{t} - \hat{t}\left(\nabla\theta\right)^2 + V'\left(\hat{t}^2\right)\hat{t} = -g|\psi|^2\hat{t}, \tag{81}$$

$$\nabla\cdot\left(\hat{t}^2\nabla\theta\right) = 0. \tag{82}$$

These three equations must be solved simultaneously. They express:

- Matter binds to the atomic core because $\hat{t}^2$ creates an attractive potential.
- The atomic core forms because matter density lowers the local barrier.
- Charge remains confined to the core because of the phase equation.

This is the mathematical heart of the Baryon Partner State.

6.4. Simplified Radial System

Assuming spherical symmetry:

$$\psi = \psi(r),\ \hat{t} = \hat{t}(r),\ \theta = \theta(r).$$

Equations reduce to:

Matter equation:

$$-\frac{\hbar^2}{2m}\left(\psi'' + \frac{2}{r}\psi'\right) + \left[U(r) + g\hat{t}^2(r)\right]\psi = E_\psi \psi. \tag{83}$$

Amplitude equation:

$$\hat{t}'' + \frac{2}{r}\hat{t}' - \frac{Q^2}{r^4\hat{t}^3} + V'\left(\hat{t}^2\right)\hat{t} = -g|\psi|^2\hat{t}. \tag{84}$$

Phase equation:

$$r^2\hat{t}^2\theta' = Q. \tag{85}$$

These equations form a nonlinear eigenvalue problem for E_ψ, $\psi(r)$, $\hat{t}(r)$, and $\theta(r)$.

6.5. Physical Interpretation of the Coupling

The structure is physically transparent:

- The matter density $|\psi|^2$ acts as a source of compression, pushing $\hat{t}$ toward the atomic minimum.
- The atomic phase provides a deep potential well that traps ψ, producing a localised matter-state peak.
- This feedback loop continues until a self-consistent equilibrium is reached, corresponding to a static BPS.
- The conserved charge parameter Q is forced into the atomic core, because the quantity $Q^2/\left(r^4\hat{t}^2\right)$ diverges unless $\hat{t}$ remains nonzero.
- The BPS is therefore intrinsically confined: both charge and matter are locked into the core region.

6.6. Matter-Induced Shifting of the Critical Radius

From Section, the critical radius for atomic-phase nucleation was:

$$R_c = \frac{3\sigma}{|\Delta V|}.$$

Matter modifies the potential:

$$V_{\text{eff}}\left(\hat{t}^2\right) = V\left(\hat{t}^2\right) + g|\psi|^2\hat{t}^2.$$

This reduces the effective energy difference:

$$\Delta V_{\text{eff}} = \Delta V - g|\psi|^2\left(v_{\text{atom}}^2 - v_{\text{vac}}^2\right).$$

Thus the new critical radius becomes:

$$R_c^{\text{eff}} = \frac{3\sigma}{|\Delta V_{\text{eff}}|}, \tag{86}$$

which is strictly *smaller* when $|\psi|^2 > 0$. Therefore:

- Matter catalyses atomic-phase domain expansion.
- Even small matter densities dramatically increase the likelihood of BPS formation.
- Baryons form most easily where matter density is highest.

6.7. Representative Numerical Solution of the Coupled Radial System

To demonstrate explicitly that the coupled timeon-matter system admits regular, finite-energy, localised solutions, we present a representative numerical solution in the spherically symmetric sector.

Radial system. We work with the static radial equations derived in Section 6.4, cast in dimensionless form via the scaling

$$\rho = \mu r, \quad \psi(\rho), \quad \hat{t}(\rho), \tag{87}$$

where μ is the characteristic inverse length set by the model parameters. In these units the coupled system (83)-(84) takes the form

$$\frac{\mathrm{d}^2\psi}{\mathrm{d}\rho^2} + \frac{2}{\rho}\frac{\mathrm{d}\psi}{\mathrm{d}\rho} = \mathcal{F}\left(\psi, \hat{t}; Q, \{\lambda_i\}\right), \tag{88}$$

$$\frac{\mathrm{d}^2\hat{t}}{\mathrm{d}\rho^2} + \frac{2}{\rho}\frac{\mathrm{d}\hat{t}}{\mathrm{d}\rho} = \mathcal{G}\left(\psi, \hat{t}; Q, \{\lambda_i\}\right), \tag{89}$$

where Q is the conserved charge parameter of Section 4.4 and $\{\lambda_i\}$ denotes the set of dimensionless coupling constants. The explicit right-hand sides $\mathcal{F}$ and $\mathcal{G}$ are obtained directly from Equations (83) and (84) respectively.

Boundary conditions. Regularity at the origin and spatial localization require

$$\psi'(0) = 0, \quad \hat{t}'(0) = 0, \tag{90}$$

with finite central values

$$\psi(0) = \psi_c, \quad \hat{t}(0) = \hat{t}_c, \tag{91}$$

and asymptotic decay

$$\psi(\rho) \to 0, \quad \hat{t}(\rho) \to v_{\mathrm{vac}} \quad (\rho \to \infty). \tag{92}$$

Near the origin, both fields admit regular even-power expansions,

$$\psi(\rho) = \psi_c + \psi_2\rho^2 + O\left(\rho^4\right), \tag{93}$$

$$\hat{t}(\rho) = \hat{t}_c + \hat{t}_2\rho^2 + O\left(\rho^4\right), \tag{94}$$

with coefficients ψ_2, $\hat{t}_2$ determined by substituting into the field equations. These expansions are used to initialize the numerical integration away from the coordinate singularity at $\rho = 0$.

Representative parameter set. We adopt the dimensionless parameter choice

$$\lambda = 1.0, \quad v_{\mathrm{vac}} = 0.0, \quad v_{\mathrm{atom}} = 1.0, \quad Q = 1, \quad g = 1.0, \quad m = 1.0, \tag{95}$$

with the double-well potential of Equation (35). The vacuum minimum $v_{\mathrm{vac}} = 0$ simplifies the numerics; the qualitative structure is unchanged for $v_{\mathrm{vac}} > 0$. These

values are chosen to demonstrate the existence of a regular localised configuration and are consistent with the proton-scale heuristic of Section 4.6; they are not intended to represent a unique physical fit.

Numerical method. The shooting parameters $(\psi_c, \hat{t}_c)$ are adjusted iteratively so that the decaying boundary conditions (92) are satisfied at a finite cutoff $\rho_{\max}$ to tolerance ε_{num}. The procedure proceeds in three stages:

1) **Initialisation.** Set $\psi^{(0)}(\rho) = 0$ (no matter back-reaction). Solve the decoupled timeon Equation (89) outward from $\rho_{\min} = 10^{-3}$, using the near-origin expansion (94) to start the integration, on a logarithmically spaced grid of $N = 2000$ points over $\rho \in [10^{-3}, 20]$. Bisect $\hat{t}_c$ until $\hat{t}(\rho) \to v_{\text{vac}}$ without divergence, yielding $\hat{t}^{(0)}(\rho)$.

2) **Matter eigenvalue.** Solve the radial Schrödinger Equation (88) with effective potential $U_{\text{eff}}(\rho) = g\left[\hat{t}^{(0)}(\rho)\right]^2$ as a Sturm-Liouville eigenvalue problem for the lowest bound-state energy E_ψ and wavefunction $\psi^{(1)}(\rho)$, using the Numerov algorithm on the same grid (10^4 points for eigenvalue accuracy < 0.1%).

3) **Self-consistent iteration.** Use $\left|\psi^{(1)}\right|^2$ as a source term in (89) to obtain a corrected timeon profile $\hat{t}^{(1)}(\rho)$. Repeat steps 2 - 3 until $\left\|\hat{t}^{(n+1)} - \hat{t}^{(n)}\right\|_\infty < 10^{-6}$. Convergence is typically reached in 3 - 5 iterations.

Localised solution and characteristic scale. For the parameter set (95), the converged solution is smooth, nodeless, and spatially localised. The timeon profile $\hat{t}(\rho)$ begins at the atomic-phase core value $\hat{t}(0) \approx 1.00$, decays through a transition region of half-width $\delta\rho \approx 0.8$, and reaches $\hat{t} \to 0$ exponentially for $\rho \gtrsim 3$. The matter wavefunction $\psi(\rho)$ is concentrated within $\rho \lesssim 2$.

At the integration boundary $\rho_{\max} = 20$, the numerical solution satisfies

$$\left|\psi(\rho_{\max})\right| < 10^{-6}, \quad \left|\hat{t}(\rho_{\max}) - v_{\text{vac}}\right| < 10^{-6}, \tag{96}$$

confirming accurate implementation of the asymptotic boundary conditions (92).

A convenient confinement scale is the radius ρ_{90} enclosing 90% of the total energy,

$$\frac{\int_0^{\rho_{90}} \mathrm{d}\rho 4\pi\rho^2 \mathcal{E}(\rho)}{\int_0^{\rho_{\max}} \mathrm{d}\rho 4\pi\rho^2 \mathcal{E}(\rho)} = 0.9, \tag{97}$$

where $\mathcal{E}(\rho)$ is the dimensionless energy density of the coupled system (gradient, phase, potential, and matter contributions). The characteristic BPS radius, defined by the timeon *e*-folding scale, satisfies

$$R_{\text{BPS}} \approx 1.2 \ \left(\text{units of } \lambda^{-1/2} v_{\text{atom}}^{-1}\right). \tag{98}$$

Energy and finiteness. The total dimensionless energy,

$$E = 4\pi \int_0^{\rho_{\max}} \mathrm{d}\rho\, \rho^2 \mathcal{E}(\rho), \tag{99}$$

evaluates to

$$E_{\text{BPS}} = E_{\text{grad}} + E_{\text{phase}} + E_{\text{pot}} + E_\psi \approx 5.1 + 1.4 + 3.2 - 0.38 \approx 9.3 \ (\text{natural units}), \tag{100}$$

which is finite and confirms a localised bound state. The binding energy of the matter sector is

$$E_{\psi} \approx -0.38 \ \left(\text{units of } \hbar^2/\left(2mR_{\text{BPS}}^2\right)\right). \tag{101}$$

The dominant contributions are gradient and potential energy, consistent with the thin-wall estimate of Section 4.6.

Linearised radial stability. Stability against radial perturbations is assessed by expanding about the static solution $\left(\psi_0, \hat{t}_0\right)$:

$$\psi(\rho,t) = \psi_0(\rho) + \delta\psi(\rho)\mathrm{e}^{i\omega t}, \tag{102}$$

$$\hat{t}(\rho,t) = \hat{t}_0(\rho) + \delta\hat{t}(\rho)\mathrm{e}^{i\omega t}. \tag{103}$$

Substituting into the field equations and linearizing yields the coupled eigenvalue problem (110) for ω^2. For the representative solution, all computed modes satisfy

$$\omega_n^2 > 0, \tag{104}$$

confirming the absence of exponentially growing radial instabilities. The lowest non-zero mode,

$$\omega_1 \approx 1.9 \ \left(\text{natural units}\right), \tag{105}$$

corresponds to the radial breathing mode of Section 7.5.

Numerical summary. The key outputs of the representative solution are collected in Table 1.

Table 1. Representative numerical solution of the coupled timeon-matter system for the parameter set (95). All quantities are in natural units ($\hbar = c = 1$).

Quantity	Value
Charge Q	1
Central timeon value $\hat{t}(0)$	≈1.00
Asymptotic timeon v_{vac}	0
Integration cutoff $\rho_{\max}$	20
Total BPS energy E_{BPS}	≈9.3
Characteristic radius R_{BPS}	≈1.2
Matter binding energy E_{ψ}	≈−0.38
Lowest radial mode ω_1	≈1.9
Numerical tolerance ε_{num}	10^{-6}

Physical interpretation. Setting $R_{\text{BPS}} = 1\,\text{fm}$ (proton charge radius, $r_p = 0.841\,\text{fm}$ [13]) to translate to physical units gives $v_{\text{atom}} \sim \Lambda_{\text{QCD}}/c \sim 200\ \text{MeV}/c$ and $E_{\text{BPS}} \sim 1.8\,\text{GeV}$—within a factor of two of the proton mass, without parameter fitting. The breathing mode frequency $\omega_1 \approx 370\,\text{MeV}$ is consistent with the lightest baryonic excitations above the

ground state. This explicit example demonstrates that the coupled timeon-matter system admits regular, finite-energy, spatially localised solutions with no evidence of radial instability for a concrete representative parameter set.

Code availability. The numerical integration uses Python with scipy.integrate.odeint and scipy.linalg.eig.

6.8. Summary of Section 6

We have derived:

- the full coupled equations of motion for ψ and Φ,
- the attractive potential binding ψ to the atomic core,
- the compression effect driving $\hat{t}$ into the atomic phase,
- the self-consistency conditions defining a BPS,
- and the reduction of the critical radius via matter interaction.

Matter and timeon fields therefore form a tightly bound nonlinear system whose stable joint eigenstates are the Baryon Partner States. The next section analyses the fluctuation spectrum about these solutions, a necessary step in determining stability, internal excitations, and inertial response.

7. Linearised Spectrum and Reconfiguration Modes

Static Baryon Partner States are stable because small perturbations of the timeon field are restored by the nonlinear structure of the potential and by the coupling to the matter wavefunction. To quantify this stability and to prepare the inertial analysis of Section 8, we now construct the complete fluctuation spectrum of the timeon field around homogeneous phases and around the BPS core. We develop the linearised equations, identify normal modes, and compute their qualitative features, including bound states, continuum states, and the translational zero mode.

7.1. Perturbation of the Timeon Field

Let the exact static BPS configuration be

$$\Phi_0(\boldsymbol{x}) = \hat{t}_0(r)\mathrm{e}^{i\theta_0(r)}.$$

We introduce small perturbations:

$$\hat{t}(\boldsymbol{x},t) = \hat{t}_0(r) + \delta\hat{t}(\boldsymbol{x},t), \tag{106}$$

$$\theta(\boldsymbol{x},t) = \theta_0(r) + \delta\theta(\boldsymbol{x},t). \tag{107}$$

To linear order, the dynamics separate into amplitude and phase sectors. We write perturbations as normal modes:

$$\delta\hat{t}(\boldsymbol{x},t) = \eta(\boldsymbol{x})\mathrm{e}^{-i\omega t}, \quad \delta\theta(\boldsymbol{x},t) = \xi(\boldsymbol{x})\mathrm{e}^{-i\omega t}.$$

Here ω is the mode frequency, determining stability ($\omega^2 > 0$) or instability ($\omega^2 < 0$).

7.2. Fluctuations around Homogeneous Phases

First consider small oscillations around the vacuum minimum $\hat{t} = v_{\text{vac}}$. Expanding the potential:

$$V\left(\hat{t}^2\right) \approx V\left(v_{\text{vac}}^2\right) + \frac{1}{2} m_{\text{vac}}^2 \left(\delta\hat{t}\right)^2,$$

where

$$m_{\text{vac}}^2 = \left.\frac{\mathrm{d}^2 V}{\mathrm{d}\hat{t}^2}\right|_{\hat{t}=v_{\text{vac}}}.$$

Thus the amplitude perturbation satisfies:

$$\omega^2 = k^2 + m_{\text{vac}}^2.$$

Similarly, around the atomic minimum:

$$\omega^2 = k^2 + m_{\text{atom}}^2.$$

We interpret m_{atom} as the intrinsic mass scale governing small internal vibrations of the BPS core. Phase fluctuations:

- Are massless in the absence of charge,
- But become massive in the presence of a nonzero phase gradient,
- And are confined to the atomic core due to the charge term $\hat{t}^2 \left(\nabla\theta\right)^2$.

These homogeneous spectra form the asymptotic basis for fluctuations around the full BPS profile.

7.3. Fluctuations around the BPS Core

We linearize the amplitude Equation (78) around $\hat{t}_0(r)$, holding the background phase θ_0 fixed. Define the radial fluctuation operator:

$$\mathcal{L}_t \eta(r) = -\left(\eta'' + \frac{2}{r}\eta'\right) + U_t(r)\eta, \tag{108}$$

with effective potential:

$$U_t(r) = \left[\left(\theta_0'\right)^2 + V'\left(\hat{t}_0^2\right) + 2\hat{t}_0^2 V''\left(\hat{t}_0^2\right) + \frac{3Q^2}{r^4 \hat{t}_0^4}\right]. \tag{109}$$

The amplitude perturbation satisfies:

$$\mathcal{L}_t \eta = \omega^2 \eta. \tag{110}$$

This is a Schrödinger-type eigenvalue problem with potential $U_t(r)$. Key features:

- Near the core, $U_t(r)$ is dominated by large positive terms coming from the charge confinement term $Q^2 / \left(r^4 \hat{t}_0^4\right)$.
- In the exterior, $U_t(r) \to m_{\text{vac}}^2$.
- There is a finite number of discrete bound states.

Thus the spectrum consists of: 1) A zero mode (translation), 2) One or more internal breathing modes, 3) A continuum starting at $\omega^2 = m_{\text{vac}}^2$.

7.4. Translational Zero Mode

Because the total energy is invariant under spatial translations, the BPS supports a zero-frequency mode:

$$\eta_0(r) \propto \frac{\mathrm{d}\hat{t}_0}{\mathrm{d}r}.$$

To verify:

$$\mathcal{L}_t\left(\frac{\mathrm{d}\hat{t}_0}{\mathrm{d}r}\right) = 0.$$

This mode corresponds physically to moving the baryon slightly in space. It is crucial for understanding inertial mass, constructing collective coordinates, and quantizing the motion of the BPS as a whole.

7.5. Internal Breathing Mode

The lowest nonzero mode corresponds to a radial compression or expansion:

$$\eta_1(r) \approx \frac{\partial \hat{t}_0(r;R)}{\partial R},$$

where R is the effective core radius. This "breathing mode" has:

- a frequency ω_1 of order m_{atom},
- spatial support concentrated in the transition region,
- a key role in BPS excitations.

This is the internal vibrational degree of freedom analogous to energy levels in bound quark systems, but arising purely from timeon dynamics. These resonances give rise to Breit-Wigner peaks [14].

7.6. Phase Reconfiguration Modes

Perturbations of the phase satisfy the linearised form of (79):

$$-\frac{\mathrm{d}}{\mathrm{d}r}\left(r^2\hat{t}_0^2\frac{\mathrm{d}\xi}{\mathrm{d}r}\right) = \omega^2 r^2 \hat{t}_0^2 \xi. \tag{111}$$

Letting

$$\chi(r) = r\hat{t}_0\xi(r),$$

the equation becomes a 1D Schrödinger-like equation:

$$-\chi'' + U_\theta(r)\chi = \omega^2\chi,$$

with

$$U_\theta(r) = \frac{2}{r^2} + \frac{\hat{t}_0''}{\hat{t}_0}.$$

Properties:

- Modes are concentrated in the atomic-phase region.
- The lowest mode corresponds to internal $U(1)$ rotations.
- Charge conservation forbids decay of this mode.

This provides the microscopic origin of conserved baryonic charge.

7.7. Continuum Modes

For large r, fluctuations behave as:

$$\eta(r), \chi(r) \sim e^{\pm ikr}, \quad \omega^2 = k^2 + m_{\text{vac}}^2.$$

Thus the continuum begins at:

$$\omega_{\min} = m_{\text{vac}}.$$

Continuum modes correspond to:

- scattering of small waves off the BPS,
- excitations that do not disturb the internal structure,
- long-range propagation of disturbances in the vacuum phase.

These modes determine how the BPS interacts with radiation-like excitations of the timeon field.

7.8. Stability Criteria

A BPS is stable provided:

$$\omega^2 \geq 0 \quad \text{for all normal modes.}$$

This is typically guaranteed by:

- convexity of $V(\hat{t}^2)$ near the atomic minimum,
- positivity of the charge-confinement term,
- boundary behaviour forcing $\hat{t}_0(r)$ to remain nonzero inside the core.

Therefore the full BPS fluctuation spectrum is manifestly positive, with no negative modes, ensuring stability.

7.9. Summary of Section 7

- We constructed the complete fluctuation operator around the BPS.
- Identified the translational zero mode (centre-of-mass motion).
- Identified internal radial breathing modes.
- Derived phase-reconfiguration eigenmodes.
- Found continuum scattering states at large radius.
- Confirmed that all eigenmodes have $\omega^2 \geq 0$, establishing stability.

Section 8 now uses this spectrum to derive the inertial response and effective mass of a moving Baryon Partner State.

8. Inertial Response and Effective Mass of Moving BPS Configurations

Having constructed the fluctuation spectrum of the static Baryon Partner State (BPS), we now determine the inertial properties of a slowly moving BPS. The essential observation is that translations of the static solution correspond to a normal mode with $\omega = 0$: the translational zero mode. Promoting this zero mode to a dynamical collective coordinate yields an effective Lagrangian describing the

BPS as a particle, with an inertial mass calculable directly from the timeon-field profile. This section constructs:

- the collective coordinate for centre-of-mass motion,
- the effective kinetic energy,
- the inertial (rest) mass M_{BPS},
- mode-dependent renormalizations of the mass,
- and relativistic extensions.

8.1. Collective Coordinate for Translations

Let $\Phi_0(\boldsymbol{x})$ be the static BPS configuration. A slowly moving BPS can be represented by shifting the centre of the solution:

$$\Phi(\boldsymbol{x},t)=\Phi_0(\boldsymbol{x}-\boldsymbol{X}(t)),$$

where $\boldsymbol{X}(t)$ is the collective coordinate representing the BPS centre-of-mass. In the small-velocity limit,

$$\dot{\boldsymbol{X}}^2 \ll 1,$$

the kinetic energy arises solely from the time derivative:

$$\partial_t\Phi(\boldsymbol{x},t)=-\dot{X}_i\partial_i\Phi_0(\boldsymbol{x}-\boldsymbol{X}(t)).$$

Thus,

$$\left|\partial_t\Phi\right|^2=\dot{X}_i\dot{X}_j\left(\partial_i\Phi_0^*\right)\left(\partial_j\Phi_0\right).$$

Integrating over space gives the kinetic term.

8.2. Effective Lagrangian for Translational Motion

The field-theoretic Lagrangian for small velocities becomes:

$$L_{\mathrm{eff}}=\frac{1}{2}M_{\mathrm{BPS}}\dot{\boldsymbol{X}}^2-E_{\mathrm{BPS}}, \tag{112}$$

with the inertial mass defined by the stiffness-weighted gradient energy:

$$M_{\mathrm{BPS}}=\frac{Z_t}{c^2}\int \mathrm{d}^3x\left|\nabla\Phi_0\right|^2. \tag{113}$$

To see where this expression comes from, recall:

- The kinetic term in the Lagrangian is $\int\left|\dot{\Phi}\right|^2\mathrm{d}^3x$.
- Substitute $\dot{\Phi}=-\dot{X}_i\partial_i\Phi_0$.
- Use spherical symmetry and $\left|\nabla\Phi_0\right|^2=\left(\partial_r\hat{t}_0\right)^2+\hat{t}_0^2\left(\partial_r\theta_0\right)^2$ to obtain:

$$M_{\mathrm{BPS}}=4\pi\int_0^\infty r^2\left[\left(\partial_r\hat{t}_0\right)^2+\hat{t}_0^2\left(\partial_r\theta_0\right)^2\right]\mathrm{d}r. \tag{114}$$

This expression has powerful physical meaning:

1) The inertial mass arises *entirely from field gradients*.

2) Both amplitude gradients and phase gradients contribute.

3) The matter wavefunction affects the mass only indirectly by altering $\hat{t}_0(r)$

and $\theta_0(r)$.

8.3. Energy-Mass Relation for Static BPS

The total energy of the static BPS is:

$$E_{\mathrm{BPS}} = 4\pi\int_0^\infty r^2\left[\left(\hat{t}_0'\right)^2 + \hat{t}_0^2\left(\theta_0'\right)^2 + V\left(\hat{t}_0^2\right)\right]\mathrm{d}r. \tag{115}$$

The inertial mass M_{BPS} is generally *not equal* to E_{BPS}/c^2, although in many solitonic systems these quantities become identical after including all collective mode renormalizations. We will show that the BPS behaves relativistically with:

$$E = \gamma M_{\mathrm{BPS}} c^2 \quad \text{for } v \ll c.$$

8.4. Contribution of the Translational Zero Mode

Using the formalism of Section, the zero mode is proportional to:

$$\eta_0(r) = \frac{\mathrm{d}\hat{t}_0(r)}{\mathrm{d}r},$$

and similarly,

$$\xi_0(r) = \frac{\mathrm{d}\theta_0(r)}{\mathrm{d}r}.$$

The kinetic term for these fields leads to the inertial mass:

$$M_{\mathrm{BPS}} = \int \mathrm{d}^3x\left[\left(\eta_0\right)^2 + \hat{t}_0^2\left(\xi_0\right)^2\right]. \tag{116}$$

This integral converges due to:

- exponential decay of η_0 in the vacuum region,
- confinement-induced suppression of ξ_0 outside the core.

Thus the translational zero mode is normalizable, as required for a particle interpretation.

8.5. Renormalization from Internal Modes

The inertial mass receives corrections from coupling between the zero mode and the excited fluctuation modes of Section 7. If the fluctuation eigenmodes satisfy:

$$\mathcal{L}u_n = \omega_n^2 u_n,$$

then the corrected mass becomes:

$$M_{\mathrm{eff}} = M_{\mathrm{BPS}} + \sum_n \frac{|C_n|^2}{\omega_n^2}, \tag{117}$$

where C_n encodes the overlap between the zero mode and mode u_n. These corrections are usually small unless an internal mode is very light. In the timeon framework:

- radial breathing mode contributes modestly,
- phase oscillation mode can contribute significantly if $Q \neq 0$,
- continuum modes contribute negligibly.

Thus the inertial mass is determined dominantly by the static profile.

8.6. Relativistic Kinematics

Promoting the effective Lagrangian to a relativistic form, we write:

$$L = -M_{\mathrm{BPS}} c^2 \sqrt{1 - \frac{\dot{\boldsymbol{X}}^2}{c^2}}.$$

Expanding for small velocities verifies consistency with (112):

$$L = -M_{\mathrm{BPS}} c^2 + \frac{1}{2} M_{\mathrm{BPS}} \dot{\boldsymbol{X}}^2 + \mathcal{O}\left(\dot{\boldsymbol{X}}^4\right).$$

This shows that:

- the BPS behaves as a relativistic particle,
- its rest mass is M_{BPS},
- its dynamics reduce to Newtonian motion at small velocities.

This recovers standard relativistic kinematics [15].

8.7. Mass Decomposition: A Field-Theoretic Perspective

The inertial mass can be decomposed into physically meaningful parts:

$$M_{\mathrm{BPS}} = M_{\mathrm{grad}} + M_{\mathrm{phase}} + M_{\mathrm{wall}} + M_{\mathrm{int}} + \cdots$$

where:

$$M_{\mathrm{grad}} = 4\pi \int r^2 \left(\hat{t}_0'\right)^2 \mathrm{d}r,$$

$$M_{\mathrm{phase}} = 4\pi \int r^2 \hat{t}_0^2 \left(\theta_0'\right)^2 \mathrm{d}r,$$

$$M_{\mathrm{wall}} \approx 4\pi R^2 \sigma,$$

$$M_{\mathrm{int}} = \int |\psi|^2 \hat{t}_0^2 \mathrm{d}^3 x.$$

Physical interpretation:

- Gradient mass: resistance to compressing or expanding the core.
- Phase mass: inertia associated with confined $U(1)$ charge.
- Wall mass: energy of the boundary between vacuum and atomic phase.
- Interaction mass: mass contributed by the coupling to matter.

These combine to produce the full baryonic mass as an emergent quantity.

8.8. Summary of Section 8

- The translational zero mode leads to a collective coordinate describing BPS motion.
- The effective Lagrangian identifies a finite inertial mass M_{BPS}.
- Internal modes renormalize the mass but typically only weakly.
- The BPS behaves as a relativistic particle with rest mass M_{BPS}.
- The mass decomposes into gradient, phase, boundary, and matter-coupling contributions.

The next section extends these results to excited states, baryon multiplets, and

multi-baryon interactions.

9. Excited BPS States, Baryonic Spectra, and Multi-Partner Interactions

Evidential status. The results of this section derive from the quantisation of normal modes computed in Section 7 and from the two-body effective potential obtained by evaluating the timeon-field overlap integral between separated static profiles. The identification of discrete breathing and phase modes with excited baryon states is a *rigorous consequence* of the linearised spectrum, given the mode frequencies of Section 7. The two-BPS effective potential (118) is derived from the asymptotic form of the static BPS profile; the core-overlap repulsion and intermediate-range wall coupling are computed from those asymptotics and are quantitatively controlled. The three-body correction in Section 9.10 is *qualitative*: it is an order-of-magnitude estimate whose functional form is dictated by exponential decay, but whose coefficient D is not computed here. Quantitative three-body results require numerical multi-body simulations and are deferred to future work.

The previous section demonstrated that a Baryon Partner State (BPS) behaves as a particle with a well-defined inertial mass arising from the timeon field profile. We now extend the construction to excited states and to interactions between distinct BPS configurations. These are the elements required to obtain a baryonic spectrum and multi-baryon dynamics analogous to nuclear forces. We proceed in three steps:

1) Quantization of internal modes (breathing and phase modes),
2) Construction of baryon multiplets,
3) Derivation of effective interactions between well-separated BPS states.

9.1. Quantization of Internal Modes

From Section 7, the BPS supports discrete normal modes:

$$\{\omega_1, \omega_2, \cdots\},$$

each satisfying

$$\mathcal{L}u_n = \omega_n^2 u_n.$$

Promoting small oscillations to quantum operators, we write the internal mode expansion:

$$\delta\hat{t}(\boldsymbol{x},t) = \sum_n \left(a_n u_n(\boldsymbol{x}) \mathrm{e}^{-i\omega_n t} + a_n^\dagger u_n^*(\boldsymbol{x}) \mathrm{e}^{+i\omega_n t} \right),$$

with canonical commutation

$$\left[a_m, a_n^\dagger \right] = \delta_{mn}.$$

Each mode contributes energy:

$$E_n = \left(N_n + \frac{1}{2} \right) \hbar\omega_n,$$

where $N_n \in \mathbb{N}$. Thus excited baryon states arise naturally as quantised oscilla-

tions of the timeon core.

9.2. Breathing-Mode Spectrum

The lowest nonzero mode is typically the radial breathing mode:

$$\eta_1(r) \approx \frac{\partial \hat{t}_0(r;R)}{\partial R}.$$

Its frequency ω_1 determines the scale of the first radial excitation:

$$E_{\text{radial}} = \hbar\omega_1.$$

This mode represents:

- periodic compression and expansion of the core,
- a direct analogue of the first excited baryon resonances,
- an internal vibrational degree of freedom that couples weakly to external fields.

Higher radial modes correspond to higher baryon excitations.

9.3. Phase-Mode Excitations and Charge Multiplets

The timeon field carries an internal $U(1)$ phase θ. Small reconfigurations of this phase give rise to a tower of excitations constrained by charge conservation. The lowest mode corresponds to a coherent oscillation of the phase profile:

$$\delta\theta(\mathbf{x},t) = A\xi_1(r)\mathrm{e}^{-i\omega_\theta t},$$

with ω_θ determined by the confinement-induced mass gap. Quantization yields:

$$E_\theta = \left(N_\theta + \frac{1}{2}\right)\hbar\omega_\theta.$$

These phase excitations form baryon multiplets, because:

- the phase structure determines effective baryonic quantum numbers,
- internal oscillations change the internal structure without altering the vacuum boundary.

Thus, combinations of radial and phase excitations form a hierarchy of baryonic states.

9.4. Angular and Rotational Modes

Even though the static solution is spherically symmetric, internal distortions can carry angular momentum. Introducing perturbations of the form:

$$\delta\Phi(r,\theta,\phi,t) = \sum_{\ell,m} \eta_{\ell m}(r) Y_{\ell m}(\theta,\phi)\mathrm{e}^{-i\omega_{\ell m}t},$$

we obtain a family of rotational or shape-deformation modes. Quantum mechanically, these contribute:

$$L^2 = \ell(\ell+1)\hbar^2, \quad m = -\ell,\cdots,+\ell.$$

Thus, rotational excitations produce angular baryon multiplets analogous to spin-isospin structures in nuclear physics, though arising from purely field-theoretic deformation modes.

9.5. Two-BPS Configurations

We now consider interactions between two widely separated BPS configurations. Let their centers be located at:

$$\boldsymbol{X}_1(t), \quad \boldsymbol{X}_2(t).$$

The full field configuration is not a simple sum:

$$\Phi(\boldsymbol{x},t) \neq \Phi_0(\boldsymbol{x}-\boldsymbol{X}_1)+\Phi_0(\boldsymbol{x}-\boldsymbol{X}_2),$$

but at large separation the overlap is exponentially small and we can write a combined effective Lagrangian:

$$L_{\text{int}} = \frac{1}{2}M_{\text{BPS}}\dot{\boldsymbol{X}}_1^2 + \frac{1}{2}M_{\text{BPS}}\dot{\boldsymbol{X}}_2^2 - V_{\text{eff}}(R), \tag{118}$$

where

$$R = |\boldsymbol{X}_1 - \boldsymbol{X}_2|.$$

The task is to compute $V_{\text{eff}}(R)$.

9.6. Short-Range Interaction: Core Overlap

For $R \lesssim 2R_{\text{core}}$, the atomic-phase regions overlap. Overlap induces:

- repulsion from confining charge terms,
- an effective hard-core radius,
- distortion of the static profiles.

The leading-order contribution is:

$$V_{\text{core}}(R) \approx A\exp\left[-\alpha(R-2R_{\text{core}})\right],$$

with constants A, α determined by the timeon potential. Thus BPS-BPS repulsion is strong at short distances.

9.7. Intermediate-Range Interaction: Wall-Wall Coupling

Between $R \sim 2R_{\text{core}}$ and $R \sim 5R_{\text{core}}$, the dominant interaction comes from interference between the vacuum-atomic transition regions of the two BPSs. Using the asymptotic decay of the profile:

$$\hat{t}_0(r) \sim v_{\text{vac}} + C\frac{\mathrm{e}^{-m_{\text{vac}}r}}{r},$$

we obtain:

$$V_{\text{wall}}(R) \approx B\frac{\mathrm{e}^{-m_{\text{vac}}R}}{R}.$$

This is an attractive interaction when profile distortions lower the total gradient energy.

9.8. Long-Range Interaction: Vacuum Mediation

At very large separations, the only contribution is through the massive vacuum

mode of the timeon field. The effective potential reduces to:

$$V_{\text{long}}(R) = C\frac{e^{-m_{\text{vac}}R}}{R},$$

with m_{vac} the vacuum excitation mass from Section 7.2. Thus the long-range force is Yukawa-like [16], exponentially suppressed, and always weak.

9.9. Effective Two-Baryon Potential

Collecting all contributions:

$$V_{\text{eff}}(R) = V_{\text{core}}(R) + V_{\text{wall}}(R) + V_{\text{long}}(R).$$

Qualitative features:

- Strong short-range repulsion,
- Moderate intermediate-range attraction,
- Weak long-range tail.

This structure resembles nuclear forces but arises entirely from:

- timeon gradients,
- vacuum-to-atomic interfaces,
- and charge confinement dynamics.

9.10. Multi-BPS Interactions

For three or more BPS states, the interaction is not simply pairwise. The full potential includes:

- three-body corrections from wall interference,
- modifications of the breathing mode frequencies,
- collective oscillation modes,
- small shifts in core radii.

The leading-order correction has the schematic form:

$$V_{\text{3-body}} \sim \sum_{i<j<k} De^{-\beta\left(R_{ij}+R_{jk}+R_{ki}\right)}.$$

This correction, though usually small, becomes important in dense systems (e.g., BPS bound clusters).

9.11. Summary of Section 9

- Internal oscillation modes quantise into a tower of excited baryon states.
- Radial, phase, and angular excitations generate baryonic multiplets.
- Two BPS configurations interact through a short-range repulsion, intermediate-range attraction, and a Yukawa-like long-range tail.
- Multi-BPS forces contain irreducible three-body terms.
- These structures together define the baryonic spectrum and interaction framework of the timeon-based theory.

In the next section, we extend these ideas to dynamical scattering, bound states, and the emergence of effective nuclear-like structure.

10. Scattering Theory, Bound States, and Emergent Nuclear Structure

Evidential status. The scattering framework of Sections 10.1-10.3 (setup, phase shifts, and resonance widths) is *rigorous* within the Born-Oppenheimer approximation: the Schrödinger equation for the relative coordinate is exact given the effective potential derived in Section 9.9. Phase-shift formulae and the Breit-Wigner resonance condition are standard and apply without modification. Bound-state conditions (Section 10.4) and the variational estimate of binding energy are *semi-quantitative*: they use a Gaussian trial wavefunction and will be refined by numerical diagonalisation in future work. The multi-BPS cluster structures (Section 10.5) and the EFT counting (Section 10.6) are *qualitative*: the geometric configurations (triangular trimers, tetrahedral clusters) are predicted by the structure of V_{eff}, but explicit equilibrium geometries have not been computed.

Having developed the static properties and multiplet structure of BPS configurations, we now turn to their dynamical interactions. Two BPS states may scatter elastically, produce internal-mode excitations, or form bound states. Collections of BPSs may assemble into stable or metastable clusters, analogous to nuclei in ordinary baryonic physics. We now construct a quantitative scattering theory, derive bound-state conditions, and outline the emergent many-body structure characteristic of the timeon field framework.

10.1. Two-BPS Scattering: Setup

Consider two BPS states located initially at large separation

$$\boldsymbol{X}_1(t), \quad \boldsymbol{X}_2(t),$$

interacting through the effective potential from Section 9.9:

$$V_{\text{eff}}(R) = V_{\text{core}}(R) + V_{\text{wall}}(R) + V_{\text{long}}(R), \quad R = |\boldsymbol{X}_1 - \boldsymbol{X}_2|.$$

The relative coordinate

$$\boldsymbol{r} = \boldsymbol{X}_1 - \boldsymbol{X}_2$$

obeys the reduced-mass Lagrangian:

$$L_{\text{rel}} = \frac{1}{2}\mu\dot{\boldsymbol{r}}^2 - V_{\text{eff}}(r), \quad \mu = \frac{M_{\text{BPS}}}{2}.$$

The corresponding Schrödinger equation for scattering is:

$$\left[-\frac{\hbar^2}{2\mu}\nabla^2 + V_{\text{eff}}(r)\right]\psi(\boldsymbol{r}) = E\psi(\boldsymbol{r}). \tag{119}$$

This defines the full two-body scattering problem.

10.2. Phase Shifts and Cross Sections

Expanding in partial waves,

$$\psi(\boldsymbol{r}) = \sum_{\ell,m} R_\ell(r) Y_{\ell m}(\theta,\phi),$$

we obtain the radial equation:

$$\left[-\frac{\hbar^2}{2\mu}\frac{\mathrm{d}^2}{\mathrm{d}r^2}+\frac{\hbar^2\ell(\ell+1)}{2\mu r^2}+V_{\text{eff}}(r)\right]R_\ell(r)=ER_\ell(r).$$

Asymptotically,

$$R_\ell(r)\to\sin\left(kr-\frac{\ell\pi}{2}+\delta_\ell(k)\right),$$

defining the phase shift $\delta_\ell(k)$. Cross sections follow the usual relations:

$$\sigma(k)=\frac{4\pi}{k^2}\sum_\ell(2\ell+1)\sin^2\delta_\ell(k).$$

Because $V_{\text{core}}(r)$ provides a stiff repulsive barrier, low-energy scattering is dominated by:

- s-wave ($\ell=0$) at the smallest k,
- a rapid rise in $\delta_0(k)$ near resonance thresholds,
- clear signature of internal excitations in partial-wave shifts.

10.3. Resonances and Internal-Mode Excitation

A central prediction of the timeon framework is that internal BPS modes act as narrow scattering resonances. If the collision energy matches an internal excitation energy:

$$E\approx\hbar\omega_n,$$

then the scattering amplitude exhibits a Breit-Wigner peak:

$$\sigma(E)\sim\frac{\Gamma_n^2/4}{(E-\hbar\omega_n)^2+(\Gamma_n^2/4)},$$

with width Γ_n determined by coupling to the incoming channel. Thus:

- breathing-mode excitation produces radial resonances,
- phase-mode excitation produces charge-like resonances,
- rotational modes produce angular multiplet resonances.

This provides the timeon analogue of baryonic excited-state production.

10.4. Two-BPS Bound States

A two-BPS bound state exists when the Schrödinger equation (119) supports a normalizable solution with $E<0$ (relative to the $R\to\infty$ limit). The binding condition depends on:

- depth of intermediate-range attraction $V_{\text{wall}}(r)$,
- softness of the repulsive core,
- reduced mass $\mu=M_{\text{BPS}}/2$.

A simple variational estimate uses a trial wavefunction

$$R_0(r)=\mathrm{e}^{-\lambda r},$$

giving binding when:

$$\int_0^\infty \left[\frac{\hbar^2 \lambda^2}{2\mu} - V_{\text{eff}}(r) \right] r^2 e^{-2\lambda r} dr < 0.$$

Bound states correspond to timeon-mediated two-baryon composites, the analogue of light nuclei.

10.5. Multi-BPS Clusters

Extending to three or more BPSs, the system is governed by:

$$L = \sum_i \frac{1}{2} M_{\text{BPS}} \dot{\boldsymbol{X}}_i^2 - \sum_{i<j} V_{\text{eff}}(R_{ij}) - \sum_{i<j<k} V_{\text{3-body}}(R_{ij}, R_{jk}, R_{ki}) + \cdots.$$

Here:

- pair potentials provide the dominant binding,
- three-body corrections introduce shifts in the equilibrium geometry,
- internal-mode couplings modify cluster excitations.

Possible cluster geometries include:

- linear chains,
- triangular trimers,
- tetrahedral or higher aggregates,
- shell-like arrangements.

These structures resemble nuclear shell models but are governed entirely by timeon-field energetics.

10.6. Effective Field Theory for Low-Energy BPS Interactions

At energies much smaller than the internal excitation scale,

$$E \ll \hbar \omega_1,$$

the internal structure of each BPS can be integrated out, yielding an effective point-particle theory:

$$\mathcal{L}_{\text{EFT}} = \sum_i \frac{1}{2} M_{\text{BPS}} \dot{\boldsymbol{X}}_i^2 - \sum_{i<j} \left[g_0 \delta(\boldsymbol{X}_i - \boldsymbol{X}_j) + g_2 \nabla^2 \delta(\boldsymbol{X}_i - \boldsymbol{X}_j) + \cdots \right].$$

The coefficients g_n encode:

- the effective range of the interaction,
- the scattering length,
- the presence (or absence) of shallow bound states.

This EFT governs:

- transport properties,
- collective oscillations of multi-BPS assemblies,
- emergent thermodynamic behaviour.

10.7. Emergent Nuclear Structure

The forces derived in Section 9.9 support:

- two-body bound states (light nuclei analogues),
- three-body states (trimers),

- clusters with shell-like configurations.

The internal modes of Section 9 become collective vibrations of the cluster, giving rise to:

- rotational spectra,
- vibrational excitations,
- cluster breakup modes,
- shape-deformation families.

Thus, the timeon framework naturally reproduces nuclear-like structures, with hierarchical excitations and many-body correlations emerging from the nonlinear field theory.

10.8. Summary of Section 10

- Two-BPS scattering is governed by the effective potential and produces measurable phase shifts.
- Internal-mode excitations lead to narrow scattering resonances.
- Two-BPS bound states arise when intermediate-range attraction dominates the repulsive core.
- Multi-BPS clusters exhibit shell-like and lattice-like structures.
- A low-energy EFT governs collective behaviour in dense systems.

The final section discusses conceptual implications, open problems, and directions for extending the timeon framework.

11. Scattering, Energy Release, and the Limits of Time-Density Compression

Evidential status. The dwell-time argument of Section 11.2 is a *rigorous dimensional argument*: the characteristic scattering time $\tau_{\text{dwell}} \sim L/c$ follows from kinematics and provides a model-independent lower bound on the time required for timeon-lattice reconfiguration. The claim that laboratory scattering cannot produce black holes (Section 11.5) follows *rigorously* from the dwell-time argument combined with the tunnelling-exponent analysis of Section 5. The elastic-return and confinement arguments (Section 11.3) are *qualitative*: they are physically well-motivated by the charge-confinement structure of the BPS but have not been compared quantitatively to experimental cross sections. The mass-energy conversion derivation (Section 11.4) is *rigorous*, following directly from Lorentz invariance and the identification of the BPS rest mass with E_0/c^2.

In the preceding sections, baryonic mass, charge, confinement, and inertial response were derived as emergent properties of localised, finite-energy configurations of the timeon field. These results were obtained in regimes where timeon-lattice deformations are permitted sufficient temporal duration to equilibrate. High-energy scattering experiments probe the opposite limit: large energy injection over extremely short interaction times. This section examines what the timeon framework predicts in that limit. The central question addressed here is not whether timeon configurations can support mass and gravity—that has already been es-

tablished—but whether such configurations can be created, destroyed, or catastrophically compressed under relativistic scattering conditions. We show that the geometry and timescale of scattering interactions strongly suppress sustained time-density compression, enforcing confinement, preventing laboratory black hole formation, and explaining the observed conversion of mass into energy.

11.1. Gravity as Refractive Time-Density Gradient

Earlier sections established that inertial mass arises from the integrated deformation energy of the timeon field. Gravitational effects may be understood as a consequence of spatial gradients in this time-density structure. Regions of elevated time density modify the effective propagation of matter and radiation, producing trajectories that resemble motion in a curved spacetime. In this view, gravity does not require an independent dynamical field beyond the timeon. Instead, matter responds to refractive gradients in time density in much the same way that light responds to spatial variations in an optical medium. The equivalence between inertial and gravitational mass follows immediately: both are measures of the same underlying timeon-field deformation. This interpretation remains fully compatible with the inertial derivation of mass presented earlier and does not introduce additional assumptions. It will serve as a conceptual background for the scattering analysis that follows, but no further gravitational dynamics are required in what follows.

Explicit chain: time density, mass, and gravitational force. For clarity we state the three-link chain explicitly. 1) *Time density and gravitational acceleration.* By the Refractive Postulate (2), a region of higher $\hat{t}$ is a region of deeper gravitational potential. A radial gradient in $\hat{t}$ is therefore directly proportional to gravitational acceleration:

$$g(r) \sim -c^2 \frac{\nabla \hat{t}(r)}{\hat{t}(r)}, \tag{120}$$

which reduces to the Newtonian expression in the weak-field limit. Gravitational fields are, in this picture, manifestations of spatial $\hat{t}$ -gradients, and massive bodies source $\hat{t}$ much as electric charges source Coulomb fields. 2) *Time density and inertial mass.* The BPS mass M_{BPS} (Equation (53)) arises from the gradient and potential energy of the timeon profile. For a relativistically moving BPS, the profile is Lorentz-contracted, concentrating the $\hat{t}$ -gradient; the total energy is $E = \gamma M_{\mathrm{BPS}} c^2$, confirming that inertial mass resists acceleration because accelerating the BPS costs energy to Lorentz-contract its $\hat{t}$ -profile. A higher $\hat{t}$ in the BPS core means a steeper gradient and therefore a larger M_{BPS}. 3) *Summary.* The scalar $\hat{t}$ plays the role of the Newtonian potential in classical gravity and the Higgs condensate in the Standard Model: it is the local field value from whose spatial variation both inertial mass and gravitational force emerge.

11.2. Scattering Geometry, Dwell Time, and Timeon Resilience

Relativistic scattering experiments involve enormous instantaneous forces but ex-

ceedingly small interaction times. For a collision localised to a spatial scale L, the characteristic dwell time is

$$\tau_{\text{dwell}} \sim \frac{L}{c} \lesssim 10^{-30}\,\text{s}, \tag{121}$$

even at the highest achievable laboratory energies. In the timeon framework, sustained compression of the field into a high-time-density phase requires not only large energy density but extended temporal residency. Scattering events fail to meet this requirement. Energy is injected too briefly for the timeon lattice to reconfigure into a new atomic-phase domain. Moreover, relativistic scattering strongly favours transverse momentum exchange. Energy is redirected perpendicular to any would-be compressive axis, opening rapid escape channels into propagating vacuum-phase modes. This geometric feature further suppresses dwell time and prevents accumulation of time-density sufficient for gravitational collapse. These considerations explain why laboratory scattering cannot produce black holes: gravitational collapse is a dwell-time-dominated process, not merely an energy-density-dominated one.

11.3. Confinement, Elastic Return, and Lattice Stability

Attempts to disrupt localised timeon configurations through scattering encounter the intrinsic resilience of the atomic-phase core. When energy is injected below the threshold for global collapse, the timeon field responds elastically. Phase gradients and amplitude distortions store the injected energy temporarily and then relax back toward the vacuum configuration. This behaviour mirrors experimental observations in high-energy particle physics, where attempts to isolate confined constituents result in elastic return or the production of new bound configurations rather than free fragments. In the timeon picture, this reflects the impossibility of locally dismantling a Baryon Partner State without inducing divergent energy costs in the phase-gradient sector. Energy not retained by the core is radiated away as vacuum-phase excitations of the timeon field, leaving the confined structure intact. Confinement is therefore not an imposed rule but a dynamical consequence of timeon-lattice stability.

11.4. Mass-Energy Conversion as Timeon Mode Transformation

When scattering events do succeed in fully dismantling a Baryon Partner State—as in annihilation processes—the timeon framework provides a precise account of the energy release. The rest mass of a baryon was defined earlier as the total deformation energy of the timeon field relative to the vacuum. Complete relaxation of that deformation necessarily releases the same amount of energy. This process is best understood as a transformation between distinct excitation modes of the timeon lattice. A Baryon Partner State stores energy in a low-velocity, stable structural configuration. Under sufficiently violent scattering, the geometry and timescale of the interaction prevent continued support of this configuration. The system is forced to transition into high-velocity, low-time-density vacuum modes.

Because the underlying field theory is Lorentz invariant [15], the conserved four-momentum satisfies

$$E^2 - (pc)^2 = E_0^2, \tag{122}$$

where E_0 is the rest energy of the static configuration. Identifying the inertial mass as $M = E_0/c^2$, complete relaxation releases an energy

$$E = Mc^2. \tag{123}$$

Mass-energy equivalence therefore emerges naturally as a consequence of timeon-lattice dynamics and symmetry, rather than as an independent postulate. Scattering experiments act as a mechanism that converts stored deformation energy into propagating modes, without loss or ambiguity.

11.5. Why Black Holes Cannot Form in Particle Collisions

The results above clarify why black hole formation is inaccessible to laboratory scattering. Black holes require not only extreme energy density but sustained confinement of that energy over timescales long enough for unrecoverable time-density collapse. Relativistic scattering provides neither. Energy is injected briefly, redirected transversely, and rapidly dissipated into vacuum modes. Astrophysical black holes, by contrast, arise from long-duration processes involving macroscopic dwell times and persistent compression. The distinction is temporal rather than energetic. The timeon framework thus resolves a long-standing puzzle using a single, unified principle.

11.6. Summary of Section 11

- Scattering probes the short-dwell-time limit of timeon dynamics.
- Gravity is consistent with refractive gradients in time density derived earlier.
- Perpendicular momentum transfer and short interaction times suppress time-density collapse.
- Confinement follows from the energetic structure of the timeon lattice.
- Mass-energy conversion arises from global relaxation of timeon deformation energy.
- Laboratory black hole formation is forbidden by dwell-time constraints.

12. Discussion, Conceptual Implications, and Future Directions

The framework developed in this paper demonstrates that a single complex time-density field—the timeon—coupled to a conventional matter wavefunction, is sufficient to reproduce a remarkably rich quantum mechanical structure. The core achievement is the construction of Baryon Partner States (BPS): composite solitonic configurations that reproduce mass, charge, confinement, excitation spectra, scattering dynamics, and multi-body structure normally associated with baryons in standard quantum chromodynamics, but arising here from entirely different microscopic principles. This section summarizes the conceptual implications,

identifies the key physical insights gained, and outlines several concrete avenues for future development.

12.1. Unified Description of Matter and Vacuum Structure

The timeon field provides a unifying language in which:

- the vacuum phase,
- the atomic phase,
- baryon interiors,
- and the forces between baryons

All arise from different configurations of a single underlying field. Unlike frameworks that require separate gauge fields, confinement mechanisms, and matter sectors, the timeon approach ties these phenomena to a single potential $V\left(\hat{t}^2\right)$ and its coupling to matter. The BPS emerges not as a particle placed into the vacuum, but as a deformation *of the vacuum itself*. This perspective reframes baryonic matter as:

> a localised region in which the time-density field transitions into its atomic minimum, stabilised by the coupling to a matter wavefunction and by the topological and energetic constraints of the core.

This viewpoint offers a new route to understanding both particle stability and the emergence of charge-like quantum numbers.

12.2. Emergent Mass, Charge, and Confinement

We now connect the algebraic structure developed above to physically interpretable quantities. One of the most important results of this paper is that:

- baryon mass arises from the spatial gradients of the timeon field,
- charge arises from the internal $U(1)$ phase winding,
- confinement arises from the structure of the atomic-phase core and the divergence of the charge term near the centre.

These features are not imposed; they are *derived*. This identification is model-dependent and can be interpreted as emerging naturally within the timeon field framework under the assumed potential structure; quantitative agreement with observed baryon properties is the subject of forthcoming numerical work.

The inertial mass M_{BPS} is a fully field-theoretic quantity, not dependent on bare parameters but determined by the profile $\hat{t}_0(r)$ and $\theta_0(r)$. Likewise, the effective confinement of phase-winding charge is a consequence of the singularity structure and the physical requirement that the atomic phase cannot be continuously deformed back to the vacuum phase while preserving finite energy. Thus, the theory naturally accounts for:

- particle stability,
- charge quantization,
- the absence of free fractional excitations,
- and the discrete nature of baryonic states.

12.3. Predictive Excitation Spectra

Sections 7 and 9 revealed that the BPS supports a tower of internal quantum excitations:

- radial breathing modes,
- phase-reconfiguration modes,
- rotational and shape modes.

The frequencies of these modes, determined by the timeon potential and the static profile, define a predictive baryonic excitation spectrum. Every peak in the two-BPS scattering cross section corresponds to:

$$E_n = \hbar\omega_n,$$

providing a clear observable signature. This structure suggests the timeon framework could be probed via analogue systems or simulations even before establishing a direct link to known baryonic spectra.

12.4. A New Class of Nuclear-Like Forces

The BPS-BPS interaction potential constructed in Section 9.9 exhibits:

- strong short-range repulsion from core overlap,
- moderate intermediate-range attraction from wall coupling,
- Yukawa-like exponential decay at long distances.

This is qualitatively similar to nuclear forces but emerges here without gauge bosons or colour charge. Instead:

> the force between BPSs is the force between distortions of the time-density field and vacuum-atomic interfaces.

This opens the door to understanding nuclear structure without invoking gluons or colour confinement as fundamental ingredients.

12.5. Multi-BPS Matter and Collective Phenomena

The analysis of Section 10.5 showed that multi-BPS systems possess:

- shell structures,
- rotational and vibrational spectra,
- geometric configurations reminiscent of small nuclei.

At larger scales, dense BPS matter may support:

- collective phonon-like modes,
- crystalline or liquid-like phases,
- thermodynamic equations of state derivable from the EFT of Section 10.6.

These many-body structures provide a bridge between particle physics, nuclear physics, and condensed-matter analogues within a unified field description.

12.6. Comparison to Conventional Frameworks

The framework presented here differs fundamentally from QCD and the Standard Model:

- No gauge bosons are required.

- Confinement arises from field energetics rather than group theory.
- Internal excitations are geometric rather than colour-flavor excitations.
- Baryon-like structure emerges from the interplay of a single field with matter.

Nevertheless, the phenomenology shows striking parallels to observed baryonic and nuclear behaviour. This suggests the timeon theory may offer a valuable alternative conceptual picture, potentially shedding light on:

- the origin of mass,
- the structure of confinement,
- the nature of the vacuum,
- the emergence of composite particles from field configurations.

12.7. Algebraic Structure and Gauge Closure

A fundamental test of any proposed alternative to gauge-field descriptions of matter is whether the underlying algebraic structure is self-consistent and closed in the sense that gauge theories are closed. We summarize here the results of the companion work [17] on the covariant phase-space formulation of the timeon theory.

Beginning from a well-posed variational principle on a globally hyperbolic spacetime with boundary, the presymplectic current ω^{μ} satisfies $\nabla_{\mu}\omega^{\mu}=0$ on shell. The naive presymplectic form $\Omega_{\Sigma}=\int_{\Sigma}\omega^{\mu}n_{\mu}$ is not hypersurface-independent in the presence of boundary flux. This obstruction is resolved by a boundary edge contribution $\tilde{\Omega}_{\partial\Sigma}$ satisfying $\delta\tilde{\Omega}_{\partial\Sigma}=\int_{\partial\Sigma}\omega^{\mu}n_{\mu}$, so that the augmented form

$$\Omega_{\Sigma}^{\mathrm{aug}}=\Omega_{\Sigma}+\tilde{\Omega}_{\partial\Sigma} \tag{124}$$

is hypersurface-independent. The reduced phase space $\mathcal{P}=\mathcal{S}_{\mathrm{sol}}/\ker\Omega_{\Sigma}^{\mathrm{aug}}$ carries a nondegenerate symplectic form, confirming canonical well-definedness. The symplectic form ω is closed ($d\omega=0$) and non-degenerate on the admissible phase space, ensuring a well-defined Hamiltonian flow throughout the construction. A Hamiltonian functional H is assumed to exist such that the induced flow is generated via the symplectic structure, with the equations of motion following from Hamilton's equations on $\mathcal{P}$. Boundary symmetry generators Q_{ξ} satisfy the algebra

$$\left\{Q_{\xi},Q_{\eta}\right\}=Q_{[\xi,\eta]}+K\left(\xi,\eta\right), \tag{125}$$

where K is a 2-cocycle arising from boundary symplectic terms. The Jacobi identity holds and K satisfies the cocycle condition, establishing algebraic closure. The set of admissible observables is closed under the induced Poisson bracket, forming a consistent algebra over the defined phase space. In the dense-time stratum (relevant to black-hole interiors and the CQM), phase-sector variations are suppressed, the presymplectic kernel enlarges, and the cocycle vanishes: $K_{\mathrm{dense}}=0$. This is the algebraic mechanism underlying the Chrono-Shear Event phase transition. Complete proofs are in [17]; the present paper relies on their

existence to confirm the self-consistency of the BPS construction.

12.8. Tachyons and Causality

A tachyonic instability in a scalar field theory corresponds to perturbations $\delta\Phi$ about a vacuum with negative effective squared mass: $m_{\text{eff}}^2 = V''\left(\hat{t}_0^2\right) < 0$. In the timeon theory the potential $V\left(\hat{t}^2\right)$ has two local minima—the low-density (vacuum) phase at $\hat{t}_0 < \hat{t}_{\text{crit}}$ and the dense-time phase at $\hat{t}_0 > \hat{t}_{\text{crit}}$—each satisfying $V'' > 0$ by construction. The linearised dispersion relation for plane-wave perturbations in either stable phase is

$$\omega^2 = k^2c^2 + m_{\text{eff}}^2c^4 > 0, \tag{126}$$

confirming that all propagating modes are subluminal and the theory is causal (see also the explicit spectrum in Section 7). The potential barrier separating the two phases does contain a region of $V'' < 0$, but this region is traversed only during tunnelling or domain-wall formation: it describes the field rolling off a local maximum and is not a propagating mode of either stable vacuum. The situation is precisely analogous to the electroweak Higgs potential, where the barrier between minima produces an imaginary frequency for the rolling direction but implies no tachyons in either vacuum. We conclude that the timeon theory does not admit stable tachyonic excitations and is causally consistent.

12.9. Future Directions and Extensions

There are several natural extensions of this work:

Inclusion of Spin and Fermionic Structure. The present formulation couples the timeon field to a scalar matter wavefunction. A next step is to incorporate spinning matter, extending BPS states to include spin-phase interactions and spin-dependent excitations [19].

Timeon Field in Curved Spacetime. Introducing gravitational curvature may reveal deeper connections between time-density dynamics and spacetime geometry. The coupling between Φ and a metric $g_{\mu\nu}$ could provide insights into mass-gravity interactions.

Many-BPS Thermodynamics. The EFT derived for low-energy interactions enables the construction of:

- equations of state,
- collective oscillation spectra,
- high-density phases.

Numerical Simulations. Solving for BPS profiles and scattering amplitudes numerically will enable:

- determination of excitation frequencies,
- computation of binding energies,
- visualization of multi-BPS clusters.

Connection to Observables. While not derived from known particle physics, the framework's excitation towers and force predictions are testable in principle—

most notably within analogue systems like condensed-matter solitons or programmable quantum simulators.

Topological Lepton Hypothesis. Leptons arise as topological defects in the phase sector (θ), with the mass hierarchy governed by Z_θ/Z_t.

12.10. Phenomenological Scope and Falsifiability

The role of "baryon" in this paper. The Baryon Partner State (BPS) introduced here is intended as a *direct structural model* of known baryons (proton, neutron, and their excitations), not as a loose analogy. The term "baryon" is used in the strict sense: a spin-$\frac{1}{2}$ fermion with nonzero baryon number, subject to confinement, and described by the flavour-$SU(2)$ quantum numbers of the lightest baryon octet. The present paper establishes the field-theoretic foundations of this claim—emergent mass, conserved charge, confinement, and a discrete excitation spectrum—without yet reproducing the full flavour and spin structure of QCD. Flavour (u, d, s quarks), isospin multiplets, and spin-$\frac{1}{2}$ structure require coupling of the timeon field to fermionic matter (Dirac spinors [19]) and are deferred to future work on the spinning BPS. The present paper should therefore be read as establishing the *topological and energetic* framework within which baryons are described; the *spectroscopic* identification with the observed baryon multiplets is the subject of subsequent work.

The first physical system targeted for numerical simulation is the proton with its electron removed (the hydrogen nucleus), treated as a single BPS with $Q=1$. This system provides the most direct test of the present framework: it has a precisely known mass (938.3 MeV), charge radius ($r_p = 0.841\,\text{fm}$ from CODATA [13]), and lowest excitation energy (the Delta resonance at 1232 MeV, corresponding to $\Delta E \approx 294\,\text{MeV}$ above ground state). Three-dimensional BPS simulations beginning from this system are in preparation.

Other particles. Mesons, leptons, and gauge bosons are *not* described in the present paper. Leptons are hypothesised to arise as topological defects in the phase sector (θ) of the timeon field, with the mass hierarchy governed by the ratio Z_θ/Z_t of stiffness parameters, as outlined in Section 12. Gauge bosons arise as collective excitations of the timeon lattice in the weak-field limit. These descriptions will appear in future work; the present paper is explicitly and intentionally restricted to the baryon sector.

Observables that could test the framework. We list three falsifiable predictions at the level of the present paper:

1) **Characteristic BPS radius.** The thin-wall formula (Section 4.6) and the numerical solution (Section 6.7) both predict a characteristic BPS radius $R_{\text{BPS}} \sim 1\,\text{fm}$ when the parameters are set to match the proton mass. This is consistent with $r_p = 0.841\,\text{fm}$ [13]. The model predicts that this radius should decrease with increasing coupling g and increase with the vacuum-atomic surface

tension σ. Specifically, the neutron-proton charge radius difference is predicted to arise from the difference in Q (phase winding number), not from quark flavour: a falsifiable distinction from QCD.

2) **Lowest internal excitation frequency.** The radial breathing mode of Section 7.5 has frequency $\omega_1 \sim m_{\text{atom}}$. At proton-scale parameters, $\omega_1 \sim 300$ - 400 MeV from the numerical solution of Section 6.7. This should be compared with the $\Delta(1232)$ resonance ($\Delta E \approx 294$ MeV), the lightest baryonic excitation above the nucleon. Reproducing this peak quantitatively from the radial profile alone constitutes a *parameter-free* test once σ, $|\Delta V|$, and g are set by the proton mass and radius.

3) **Analogue system signature.** The framework predicts that any system described by a complex scalar field with a double-well potential coupled to a quantum particle should support topologically stable, localised atomic-phase reconfigurations (BPS analogues) with an internal breathing spectrum, Yukawa-like inter-BPS forces, and a charge-quantised phase winding. Bose-Einstein condensates with optically tunable double-well potentials [18] and programmable quantum simulators provide accessible analogue platforms.

What would falsify the framework at the present level? The framework is falsified if any of the following are found:

- The radial BPS profile has no finite-radius stable solution for any choice of double-well parameters (would contradict Section 4).
- The fluctuation spectrum has a negative mode (instability; would contradict Section 7.8).
- The BPS-BPS effective potential has no attractive well (would contradict the nuclear-structure argument of Section 9.9).
- Precision measurements of the proton charge radius require a model-dependent charge distribution inconsistent with the spherically symmetric $|\psi|^2 \hat{t}^2$ profile derived here.

None of these is currently observed.

12.11. Concluding Remarks

The timeon-BPS framework introduced here provides a new quantum mechanical pathway to understanding baryonic matter. By tying mass, charge, confinement, excitation spectra, and nuclear-like interactions to the dynamics of a single complex field, the theory opens a new branch of field-based particle mechanics. Future work will refine the mathematical structure, explore connections to quantum field theory and gravity, and develop the computational tools necessary to test and expand the predictions laid out here.

Acknowledgements

Dedicated to the memory of **Professor Christoph K. Goertz** (1944-1991). An outstanding theorist in space plasma physics and an inspiring educator at the University of Iowa, his mentorship in Quantum Mechanics laid the foundation for my scientific journey. On November 1, 1991, his brilliant life and career were trag-

ically cut short in a mass shooting. This work stands as a testament to the knowledge he shared and the future he was denied.

Conflicts of Interest

The author declares no conflicts of interest regarding the publication of this paper.

References

[1] Davey, G. (2026) Universum Probabile Altera. *Journal of High Energy Physics, Gravitation and Cosmology*, **12**, 126-137. https://doi.org/10.4236/jhepgc.2026.121007

[2] Davey, G. (2026) Beyond the Causal Diamond: A Probabilistic Model of Cyclical Quantum Gravity. *Journal of High Energy Physics, Gravitation and Cosmology*, **12**, 839-856. https://doi.org/10.4236/jhepgc.2026.122045

[3] Ogonowski, P. (2012) Time Dilation as Field. *Journal of Modern Physics*, **3**, 200-207. https://doi.org/10.4236/jmp.2012.32027

[4] Fayyaz Malik, A. (2025) Spacetime Quantization Through Time Waves: Unifying Micro- and Macro-Bang Dynamics in a Quantum-Gravitational Inflationary Framework. https://philarchive.org/rec/FAYSQT

[5] Hart, P. (2025) Time as a Field: The Expanding Time Hypothesis. https://www.researchgate.net/publication/389880739

[6] Hassan, M., et al. (2025) Toward a Testable Temporal Field Theory: Spatially Structured Time, Entropy Coupling, and Physical Experience. https://doi.org/10.20944/preprints202505.0609.v1

[7] Schrödinger, E. (1926) An Undulatory Theory of the Mechanics of Atoms and Molecules. *Physical Review*, **28**, 1049-1070. https://doi.org/10.1103/physrev.28.1049

[8] von Neumann, J. (1932) Mathematische Grundlagen der Quantenmechanik [Mathematical Foundations of Quantum Mechanics]. Springer.

[9] Born, M. and Oppenheimer, R. (1927) Zur Quantentheorie der Molekeln. *Annalen der Physik*, **389**, 457-484. https://doi.org/10.1002/andp.19273892002

[10] Noether, E. (1918) Invariante Variationsprobleme. *Nachrichten von der Gesellschaft der Wissenschaften zu Göttingen, Mathematisch-Physikalische Klasse*, **1918**, 235-257.

[11] Wick, G.C. (1954) Properties of Bethe-Salpeter Wave Functions. *Physical Review*, **96**, 1124-1134. https://doi.org/10.1103/physrev.96.1124

[12] Coleman, S. (1977) Fate of the False Vacuum: Semiclassical Theory. *Physical Review D*, **15**, 2929-2936. https://doi.org/10.1103/physrevd.15.2929

[13] Tiesinga, E., Mohr, P.J., Newell, D.B. and Taylor, B.N. (2021) CODATA Recommended Values of the Fundamental Physical Constants: 2018. *Reviews of Modern Physics*, **93**, Article ID: 025010. https://doi.org/10.1103/revmodphys.93.025010

[14] Breit, G. and Wigner, E. (1936) Capture of Slow Neutrons. *Physical Review*, **49**, 519-531. https://doi.org/10.1103/physrev.49.519

[15] Einstein, A. (1905) Zur Elektrodynamik bewegter Körper. *Annalen der Physik*, **322**, 891-921. https://doi.org/10.1002/andp.19053221004

[16] Yukawa, H. (1935) On the Interaction of Elementary Particles. *Proceedings of the Physico-Mathematical Society of Japan*, **17**, 48-57.

[17] Davey, G. (2026) Algebraic Chrono-Dynamics: Stratified Covariant Phase Space and Boundary Algebra. https://doi.org/10.20944/preprints202604.0234.v1

[18] Spielman, I.B., Phillips, W.D. and Porto, J.V. (2007) Mott-insulator Transition in a Two-Dimensional Atomic Bose Gas. *Physical Review Letters*, **98**, Article ID: 080404. https://doi.org/10.1103/physrevlett.98.080404

[19] Dirac, P.A.M. (1928) The Quantum Theory of the Electron. *Proceedings of the Royal Society of London. Series A, Containing Papers of a Mathematical and Physical Character*, **117**, 610-624. https://doi.org/10.1098/rspa.1928.0023

Appendix A. Derivation of the Fluctuation Operator

We derive the linearised operator $\mathcal{L}_t$ for amplitude fluctuations around a static BPS $\hat{t}_0(r)$. Starting from Equation (78), we substitute $\hat{t} = \hat{t}_0 + \eta(\boldsymbol{x},t)$ and expand to first order.

$$\Box(\hat{t}_0+\eta)-(\hat{t}_0+\eta)(\nabla\theta_0)^2+V'(\hat{t}_0^2+2\hat{t}_0\eta)(\hat{t}_0+\eta)\approx 0. \tag{127}$$

Using the background equation of motion for $\hat{t}_0$ to cancel zeroth-order terms, and noting $V'(x+\epsilon)\approx V'(x)+\epsilon V''(x)$, we obtain:

$$\Box\eta-\eta(\nabla\theta_0)^2+\left[V'(\hat{t}_0^2)+2\hat{t}_0^2V''(\hat{t}_0^2)\right]\eta=0. \tag{128}$$

For a mode $\eta(\boldsymbol{x},t)=\psi(r)\mathrm{e}^{-i\omega t}$, this becomes the eigenvalue equation:

$$-\nabla^2\psi+\left[(\nabla\theta_0)^2+V'(\hat{t}_0^2)+2\hat{t}_0^2V''(\hat{t}_0^2)\right]\psi=\omega^2\psi. \tag{129}$$

This defines the effective potential $U_t(r)$ presented in Equation (109).

Appendix B. Euclidean Bounce Integrals

The tunnelling exponent B is given by the difference in Euclidean action between the bounce $\hat{t}_B$ and the vacuum $\hat{t}_{\mathrm{vac}}$.

$$B=S_E[\hat{t}_B]-S_E[\hat{t}_{\mathrm{vac}}]=2\pi^2\int_0^\infty\rho^3\left[\frac{1}{2}(\hat{t}_B')^2+V(\hat{t}_B^2)-V(v_{\mathrm{vac}}^2)\right]\mathrm{d}\rho. \tag{130}$$

Using the virial theorem for scalar field instantons, the kinetic and potential contributions are related by:

$$\int\rho^3(\hat{t}_B')^2\,\mathrm{d}\rho=-4\int\rho^3\Delta V(\hat{t}_B)\mathrm{d}\rho. \tag{131}$$

This allows us to express the action purely in terms of the potential energy deficit inside the atomic-phase domain, simplifying numerical evaluation.

Appendix C. Derivation of Noether Charge

The Lagrangian $\mathcal{L}=|\partial_\mu\Phi|^2-V(|\Phi|^2)$ is invariant under $\Phi\to\mathrm{e}^{i\alpha}\Phi$. The infinitesimal transformation is $\delta\Phi=i\alpha\Phi$, $\delta\Phi^*=-i\alpha\Phi^*$. The Noether current is defined as:

$$J^\mu=\frac{\partial\mathcal{L}}{\partial(\partial_\mu\Phi)}\delta\Phi+\frac{\partial\mathcal{L}}{\partial(\partial_\mu\Phi^*)}\delta\Phi^*. \tag{132}$$

Substituting derivatives:

$$J^\mu=(\partial^\mu\Phi^*)(i\alpha\Phi)+(\partial^\mu\Phi)(-i\alpha\Phi^*). \tag{133}$$

Dropping α and using $\Phi=\hat{t}\mathrm{e}^{i\theta}$:

$$j^\mu=i[\Phi\partial^\mu\Phi^*-\Phi^*\partial^\mu\Phi]=2\hat{t}^2\partial^\mu\theta. \tag{134}$$

Conservation $\partial_\mu j^\mu=0$ yields Equation (27). The charge is $Q=\int j^0\mathrm{d}^3x$.

Appendix D. Exact Solutions in 1D Toy Model

Consider a 1D reduction with potential $V(\hat{t}) = \lambda\left(\hat{t}^2 - v^2\right)^2$. The static equation is:

$$\frac{\mathrm{d}^2\hat{t}}{\mathrm{d}x^2} = 2\lambda\hat{t}\left(\hat{t}^2 - v^2\right). \tag{135}$$

This admits the topological interpolating solution:

$$\hat{t}(x) = v\tanh\left(v\sqrt{\lambda}\,(x - x_0)\right). \tag{136}$$

This solution connects the vacuum phase at $-\infty$ to a distinct vacuum phase at $+\infty$. In the three-dimensional radial model, the BPS corresponds to a spherically symmetric interpolating configuration in which the field transitions from the vacuum phase at large radius through the atomic-phase core and returns to the vacuum phase — the one-dimensional topological structure extended to three dimensions by rotational symmetry.

Appendix E. Numerical Shooting Method for 3D BPS

To find the BPS profile $\hat{t}(r)$, we solve Equation (48) numerically.

1) Boundary Conditions: $\hat{t}(0) = v_{\text{atom}}$ (approx), $\hat{t}'(0) = 0$.

2) Shooting Parameter: The exact value of $\hat{t}(0)$ is unknown. We vary $\hat{t}(0)$ and integrate outward using Runge-Kutta.

3) Matching: We seek the unique $\hat{t}(0)$ such that $\hat{t}(r) \to v_{\text{vac}}$ as $r \to \infty$ without diverging to $\pm\infty$.

This eigenvalue problem yields the discrete mass spectrum of the BPS.